Monte Carlo Simulations of a Moving Target during Spot-Scanning Particle Therapy with Protons

Vegard Schei Haraldsen

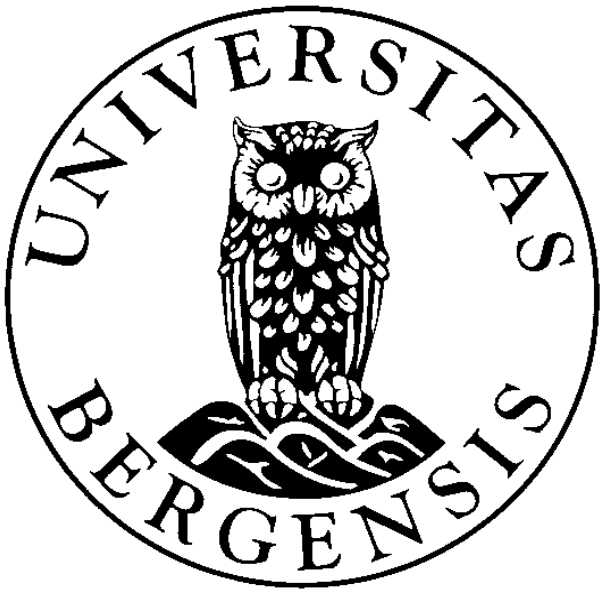

Master thesis

Department of Physics and Technology

May 2015

Acknowledgments

First I would like to thank my supervisor Professor Dieter Röhrich for guidance in the formation of the thesis, clarification and help with formulation of the simulations.

I would also like to thank Dr. Scient. Odd Harald Odland for providing me with a clinical perspective of this work and putting me in contact with personnel at Haukeland sykehus.

Thanks to Helge Pedersen for introducing me to Geant4 and how to work with it. Thanks to Boris Wagner for resolving more than one computer issue and help in setting up the data analysis with ROOT. (ROOT and computing)

Many thanks to Kristian Austreim, without your help in staying connected to my office computer the last weekend before deadline this thesis would not be in the form it is today.

Thanks to my colleagues at the nuclear physics group for pleasant company and times.

Finally, I want to thank my friends and family for their patience and support through this work, as well as encouraging words and reassuring messages during the last stretch of writing.

Abstract

During radiation therapy for cancer, the dose distribution delivered to patients will be affected by the motion of the target volume and the motion of the surrounding tissue and organs.

The overall objective of this thesis has been to investigate how the motion of the target volume affects the distribution delivered during spot-scanning particle therapy. This has been investigated with Monte Carlo simulations of a target volume moving step vise between beam spots delivered to the target volume with a proton beam. The Monte Carlo simulations were conducted with the Geant4 Toolkit, version 10.0 patch-02, and with the QGSP_BERT_HP physics list. A detector target volume measuring 20x20x4 mm was placed within a 30x30x30 cm water phantom and moved in accordance to a simple breathing cycle and average motions between irradiation of the beam spots. 25 beam spots from a circular proton beam of radius 2 mm and energy 145,60 MeV, gauss distributed with a 0,1456 MeV standard deviation, was delivered to the target. In total the beam delivered $25*10^7$ protons to the phantom. In addition to the effect of simple motion on the dose distribution, the effect of repainting within spill, delivering the dose during a gating window and re-scanning the target, was investigated.

The results of the simulations indicate that movement in the beam direction and in the secondary scanning direction, had the most detrimental effect on the dose distribution. The repainting simulations indicate that repainting within a spill average out the effect of the target and beam moving simultaneously, so called interplay effects, letting the dose distribution keep its overall shape. The gating simulations indicate that reducing the magnitude of the target movement, by delivering the dose in a specific part of the breathing cycle, increase the successful delivery of the dose distribution to the target.

With movement in the gating window, repainting within spill also lead to an increase in coverage of the CTV when the target was moved in the primary scanning direction. The result that repainting leads to a similar distribution and coverage of the CTV regardless of the direction of the target motion, the only difference being the direction of displacement, that was arrived at earlier. Leads to the conclusion that, a repaint simulation of the target moving in the secondary scanning direction in the gating window, should grant similar results to those of repainting of the target moving in the primary beam direction. The full treatment simulations show motion of the magnitude in the breathing cycle used, lead to an unacceptable dose coverage. This is in line with expectation and is consistent with the ICRU recommendations for maximum motion amplitudes in tumors to be treated with spot-scanning.

Contents

1. Radiation Therapy

Radiation Therapy is the practice of using radiation for treatment of a patient, most

often the treatment of cancer which is what the author shall be referring to hence forth. The goal of the treatment is to deliver a dose to the patient, that is sufficient to kill the cancerous tissue. While at the same time sparing the surrounding normal tissue from as much dose as possible.

From this we get the two terms Tumor Control Probability (TCP), and Normal Tissue Complication Probability (NTCP). The goal is to deliver the prescribed dose to the cancerous tissue, maximizing the TCP. While at the same time minimizing the dose to healthy tissue and with it the NTCP. Since its impossible to deliver zero dose to healthy tissue during radiation therapy treatment with external beams, a compromise must be made with the aim of reducing the chance of adverse later life effects as a consequence of the treatment.

This gives a “window” for treatment, called the therapeutic window, where the TCP dose response is higher than the NTCP. Most advances in radiation therapy revolve around widening the therapeutic window. Some examples include, more precise dose delivery and delivering the dose from multiple angles so that the dose delivered to the normal tissue is spread out over a bigger volume while the target still get the prescribed dose. (Ytre-Hauge, 2013, see other sources therein)

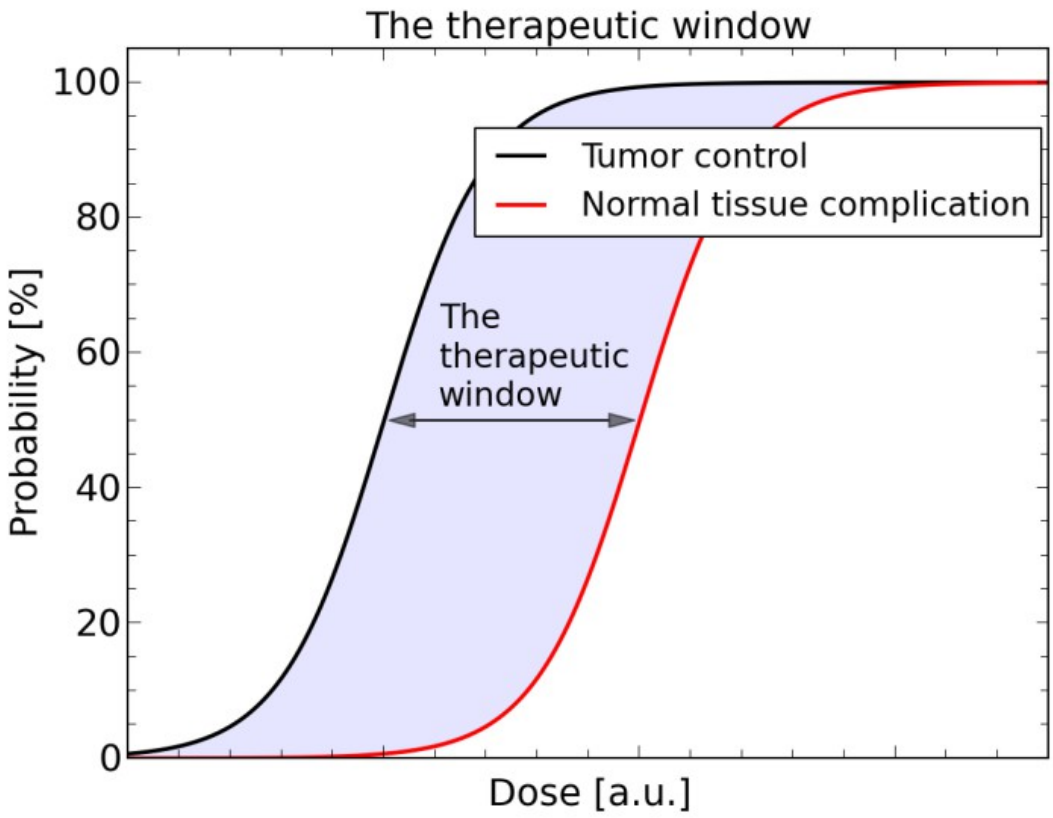

Figure 1.1: The figure shows the interplay between the tumor control probability curve and the normal tissue complication curve, that gives rise to the therapeutic window (Ytre-Hauge, 2013, see other sources therein.)

1.1 Particle Therapy

Particle therapy or hadron therapy is a treatment that radiates a patient from an external source with particles like protons or ions such as helium, carbon or oxygen. Currently particle therapy is dominated by Proton therapy with Carbon therapy being the representative for heavier ions. In this text Particle therapy will often be refereed to as proton therapy.

Particle therapy has grown into a cutting-edge clinical modality and there has been an exponential growth in proton therapy centers since the foundation of the treatment was laid by Robert Wilson in 1946. So far around 100,000 patients have been treated world wide since proton therapy took its first step into hospitals in 1990. While for carbon ions, approximately 15000 patients worldwide, but mostly in Japan, has been

treated.(NuPECC 2014)

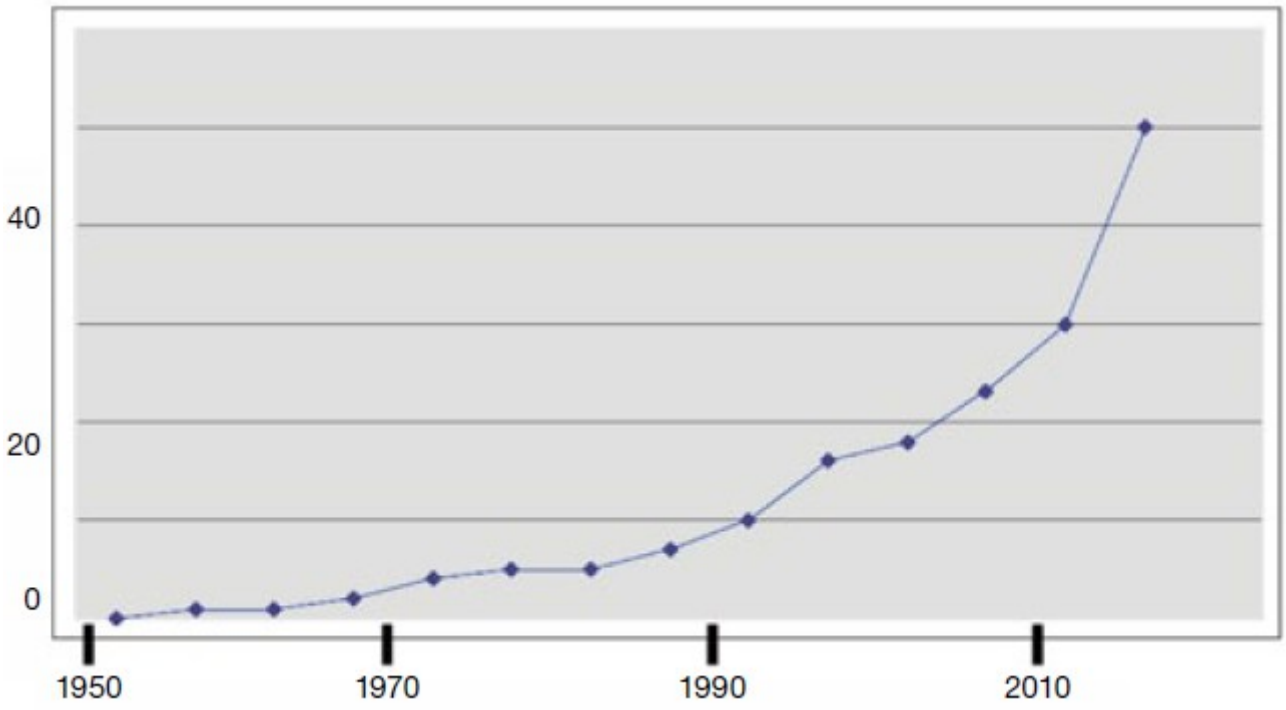

Figure 1.1.1: The increase in proton therapy centers around the world from 1950 and 2015. (NuPECC, 2014)

The reason for the interest in particle beams as a cancer treatment is based on the way a charged particles deposits its energy while traveling through matter. An ion transfers only a fraction of its energy when it collides and is only deflected a little from its original path. And while particle beams will always widen as the travel through matter, this gives protons, and other heavier ions, good ballistic properties that can be exploited to make more accurate dose plans for patients. A proton beam will have a higher lateral spread of the beam when compared to carbons, showing that a beam comprised of heavier ions have better accuracy laterally, see figure 1.1.3. (Ytre-Hauge, 2013)

In addition to this ions have a very distinct way of depositing their energy (dose). Ions deposit their energy in accordance with the Bethe Bloch formula (seen under), which shows that the average energy loss per length will increase as the velocity of

the particle decrease.

$$-\frac{dE}{dx} = 2\pi N_a r_e^2 m_e c^2 \rho \frac{Z}{A}\frac{z^2}{\beta^2}\left[ln\left(\frac{2m_e\gamma^2 v^2 W_{max}}{I^2}\right) - 2\beta^2 - \delta - 2\frac{C}{Z}\right]$$

The terms in this formula are as follows. dE/dx is the energy loss per length, also referred to as the stopping power of the particle. N_a is an abbreviation for Avogadro's number, r_e is the abbreviation for the classical electron radius and m_e denote the electron mass. ρ stands for the density of the absorbing material, while Z denote the atomic number of the absorbing material and A the atomic weight of the same. z should be understood to be the charge of the incident particle in units of e, while β is the abbreviation of v/c where v is the speed of the particle and c the speed of light. γ is the abbreviation of 1 over the root of 1 minus β^2, while W_{max} is the maximum energy transfer in a single collision and I is the mean excitation potential. Finaly δ is a density correction factor and C is a shell correction factor.

This important relation is the cause of the distinct way that ions deposits their energy (dose) when traveling through matter, where the particle deposits some energy initially at a fairly linear rate increasing with depth before losing enough velocity to start depositing much of its energy in a sharp spike with a very sharp drop in energy (dose) deposition after the spike, see figure 1.1.2.

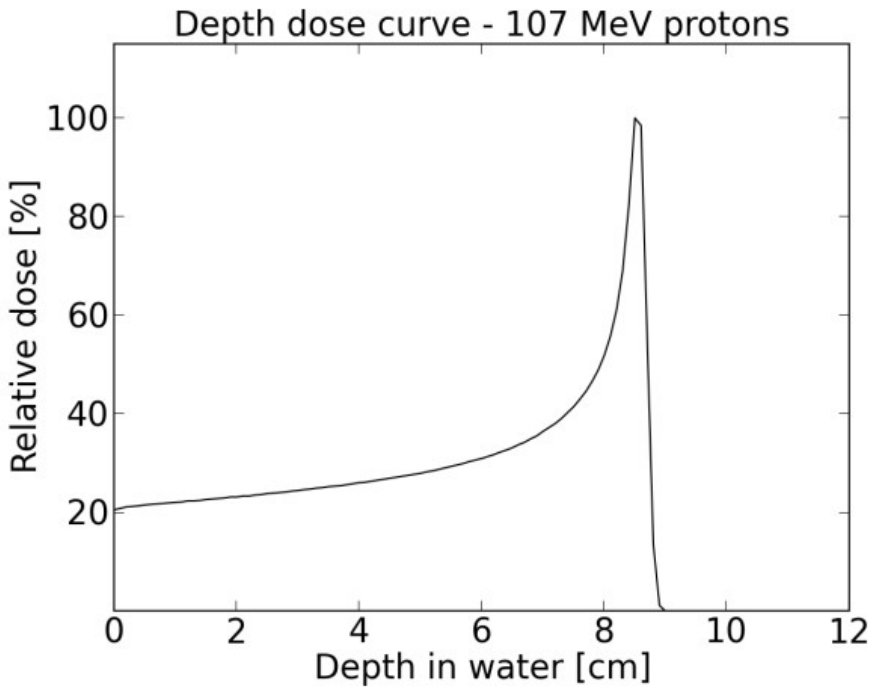

Figure 1.1.2: A plot of the dose deposition of a 107 MeV proton beam in water. (Ytre-Hauge, 2013)

This spike in the plot of energy (dose) deposition against depth in matter is called the Bragg peak after its discoverer. In therapy this behavior is exploited to deliver the prescribed dose to the patient while reducing the dose to normal tissue in comparison to treatments such as photon therapy. The reduction in integral dose to the patient may be a factor 2-3 lower typically, if compared with a similar photon treatment. (Ytre-Hauge, 2013)

While protons have almost no dose deposit after the Bragg peak, heavier ions represented by carbon ions have a probability to fragment into lighter ions as they travel through matter. Because of their lower charge the light ions produced by the fragmentation will have a longer range in accordance with the Bethe Bloch formula which lead to carbon beams having a tail of dose deposit located after the Bragg peak. (Ytre-Hauge, 2013)

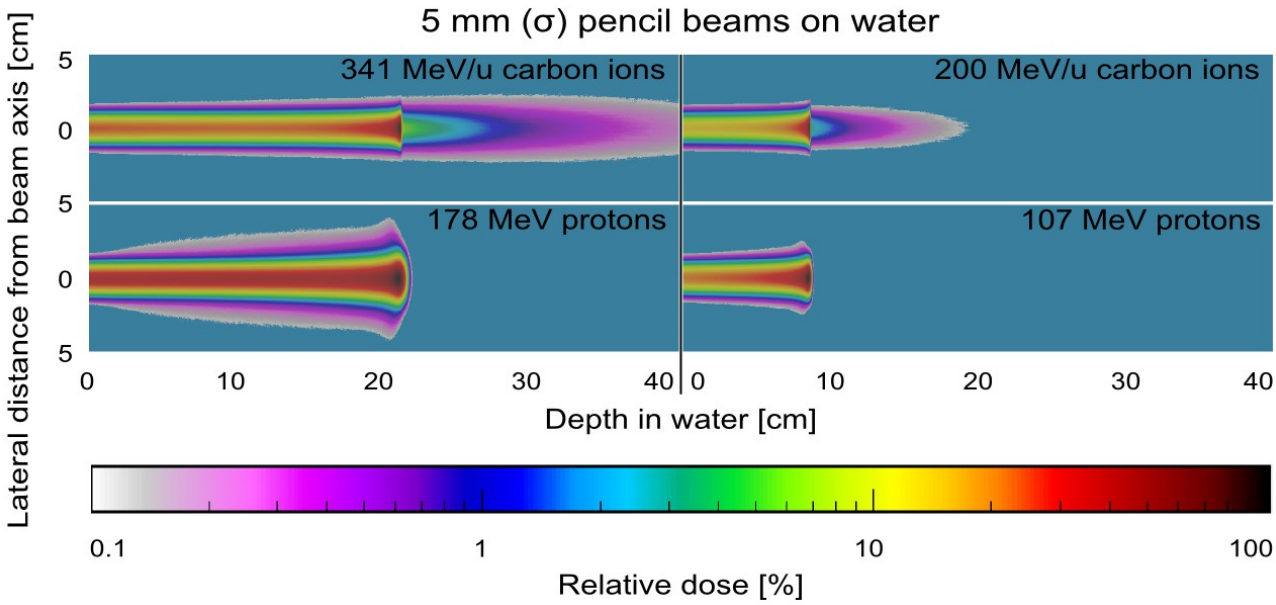

Figure 1.1.3: Monte Carlo simulations illustration the lateral spread of proton and carbon beams with depth in water. The figures also show the dose tail from fragmentation in the carbon beam. (Ytre-Hauge, 2013)

1.1.1 Accelerators

Proton therapy requires an accelerator to produce beams with high enough energies for the use in treatment. To be able to reach all positions in the human body the accelerator needs to be able to produce beams of up to, approximately, 230 MeV.

Proton therapy could therefor not fully start until the 1950s when the synchro-cyclotron made it possible to reach this energy requirement for deep seated tumors. The first patient was treated with protons in 1954 at Berkeley in the USA. Also in the USA, at Harvard University, the first dedicated proton therapy facility started to operate in 1961. This facility had a 160 MeV synchro-cyclotron accelerator and continued to treat patients until 2002. It was also here that the passive scattering technique that is still used in a majority of proton therapy facilities around the world was developed. The reason for developing this technique was the beam characteristics of the synchro-cyclotron, the beam size had to be strongly increased and the fixed energy of the beam had to be spread out to create a dose-depth distribution. This

particular accelerator was also only suitable for static tumors (brain tumors). (NuPECC, 2014)

The advancement of synchrotrons for medical purposes was driven by radio-biological research into heavier ions. The treatment of tumors with heavier ions than protons has been very promising and has led to efforts, especially in Europe and Japan, to develop synchrotrons that are suitable for clinical treatment centers, synchrotrons dedicated to carbons in particular. And while most proton facilities use compact isochronous cyclotrons, some do use synchrotrons. (NuPECC, 2014)

In recent years the introduction of highly advanced computer controlled accelerators has led to the development of much more sophisticated irradiation techniques. One such technique is the spot-scanning technique, where the narrow beam from the accelerator is actively scanned over target with the help of magnets. This technique has been pioneered at PSI and GSI since the mid-1990s and is now being transitioned into clinical treatment centers and replacing the aforementioned passive scattering technique.

These advances in technology also allows the energy of the beam extracted from a synchrotron to be varied from pulse to pulse, and even within one pulse. This then allows the direct control of the depth of the Bragg peak and, when combined with the spot-scanning technique, allows for a volume scan of the target. This technique was developed at GSI and is being applied to other synchrotron based facilities around the world for both carbon and proton therapy.

Since the beam from Cyclotrons has a fixed energy it is impossible to change the penetration depth of the beam. This is the main disadvantage of cyclotrons over the synchrotron. This is however fixed with an energy degrader of variable thickness and an energy analysis system that with the use of several magnets can tune the energy to

the values required for that particular treatment. This produces neutron radiation so the degrader is therefor typically far from the treatment room. Despite the need for external energy modulation, the degrader are fast enough to vary the range in steps of 5 mm in less than 100 ms. Since this is significantly shorter than the typical respiratory cycle of 2-4 seconds it becomes possible to use treatment techniques controlled by the patients breathing cycle. (NuPECC, 2014)

The main advantages of cyclotrons over synchrotrons is the lower cost, both of the system and the operation of it, and the size. With the use of superconducting technology it is possible to build compact cyclotrons, while a typical synchrotron have dimensions of 10 m for protons and 30 m for carbons. Cyclotrons can also produce beams that can be turned on and off rapidly, and have high and controllable intensity that can be adjusted on a time scale of milliseconds with good stability. (NuPECC, 2014)

Figure 1.1.1.1: Commercial accelerators for proton therapy, the IBA and Varian/Accel accelerators are examples of cyclotrons while the Mitsubishi and Hitachi accelerators are examples of synchrotrons. (From U. Amaldi et al. 2010.)

1.1.2 Passive scattering

The passive scattering technique was the early solution for delivering the very narrow proton beam with fixed energy to a volume of cancerous tissue. This is done by placing specific mechanical devices in the beam trajectory to shape the beam. The beam is first scattered, making it fan out from its original narrow Gaussian and form a wide homogeneously distributed beam. The beam also hits a range modulator. This is a mechanical device the rotates to change the thickness that the beam travels through, effectively reducing the energy of the protons at different rates resulting in a Spread-Out Bragg Peak. Finally the beam goes through a patient specific collimator that dose the last shaping of the beam before it enters the patient, this to better conform the beam to the targeted volume.

This early technique dose have some drawbacks though. When the beam travels through the various components that shape the beam it will also produce neutrons which will add to the dose the patient receives. The technique also requires a patient specific collimator that has to be custom made to the target volume of the patient and, even with this addition, the technique is not optimal in terms of dose deposition often having regions of extra dose in front of the target (see figure). This is rooted in the fact that in the passive scattering technique the beam energy is decreased from a maximum. There isn't really any way of removing low energy beams that hits in front of the target. The dose can therefor not conform to the target volume to the same degree that can be achieved with the more recent techniques using spot-scanning. (NuPECC, 2014)

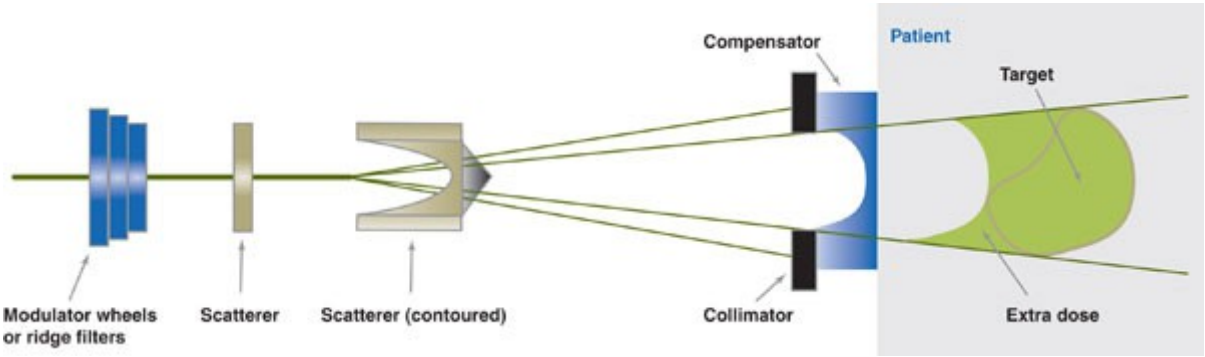

Figure 1.1.2.1: A simple illustration of the components necessary for the passive scattering technique, note the extra dose regions in front of the target.(medicalphysicsweb.org, 2010)

1.1.3 Scanning technique

When using the scanning technique the target volume is separated into slices on which beam spots are chosen. The beam is taken directly from the beam line without the use of any scattering filters or a collimator. This means that only the narrow particle beam is used. Beams have typically a size of 3-10 mm and are used to irradiate the predetermined beam spots. This is achieved with the use of magnetic fields to control where the beam hits the target in the x and y directions and by changing the energy to adjust the position of the Bragg peak. The beam irradiates a beam spot for a minimum of 1 ms (and sometimes up to 10 ms (Yupeng et al. 2014)) and is then moved to the next spot and so on and so on in a scanning manner. (NuPECC, 2014)

This makes it possible to have a much higher dose conformity to the target and thus reducing the dose to normal tissue in comparison to techniques that crate a dose field. It also dose not require any patient specific equipment or scattering filters which reduces the neutron dose significantly. (NuPECC, 2014)

However the complexity of such a scanning treatment is very high and it is highly sensitive to motion of the target. In 1993 ICRU recommended not using scanning techniques to deliver a dose to a target if the motion of the target had a motion amplitude that was greater then 10 mm. (Kraus et.al, 2011, see further references therein.) This is rooted in the inescapable fact that if you miss slightly with a dose distribution that conforms closely with the actual volume of the target, then you do not deliver the prescribed dose to the entire target volume. The more accurate a treatment is, the more severe is the effect of missing.

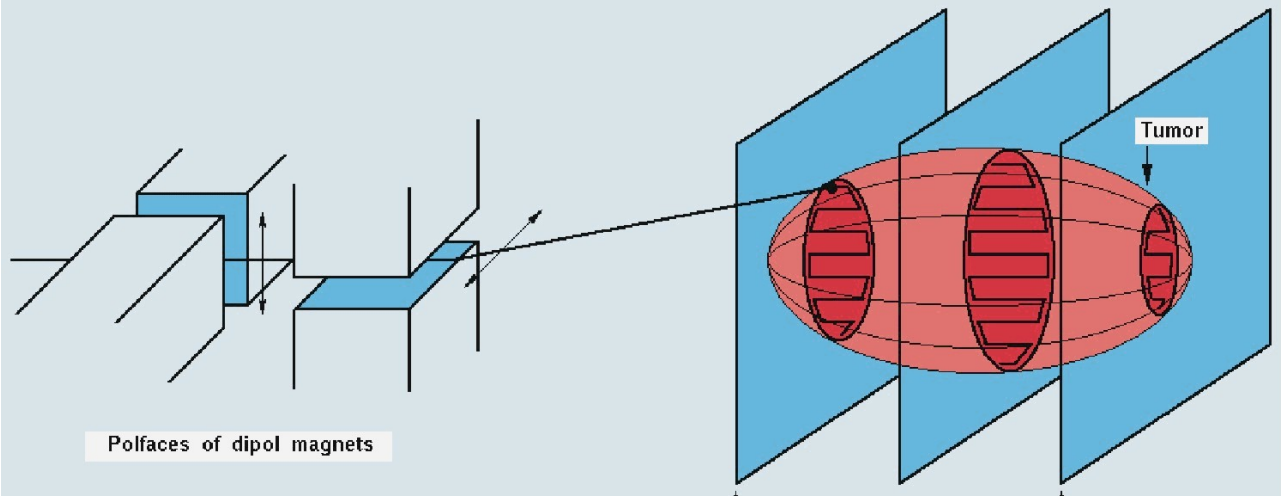

Figure 1.1.3.1: A simple illustration of the scanning technique.(From https://web-docs.gsi.de/~thdev/rt99/rt99_therapy.html)

1.2 Organ movement

All Organ motion can lead the actual received absorbed dose distribution to differ from the planned absorbed dose distribution. This leads to two scenarios of importance. That the target tumor volume is insufficiently covered, leading to an under-dosage of the tumor volume, and over-dosage of the normal tissue. Both of these scenarios can compromise the treatment. (Langen and Jones, 2001)

When considering the movement of organs in relation to radiation therapy, the many different contributing factors are divided into either intrafractional motion, interfractional or position-related organ motion (Langen and Jones, 2001). Intrafractional motion are organ movements on the time scale of seconds, the same as the irradiation of the patient, while interfractional motion are organ movements that are on the time scale of minutes and even up to days. (NuPECC, 2014)

Position-related organ motion is motion caused by a change in the patient position and it comes in to play when the patient position used during the planning scan differ from the position used during treatment. The change in patient position can lead to significant changes in organ position, especially in the thorax (chest) and abdominal region. In addition to this, the shape and thickness of the internal structures can also change. Position-related motion can be eliminated if the planing scan(s) are preformed with the patient in the treatment position. (Langen and Jones, 2001)

Cancer in organs that is affected by the motion of breathing (intrafractional), such as lung and liver cancers, are also cancers that have a very poor prognosis. Lung and liver cancer in particular is responsible for a considerable fraction of deaths by cancer today. But the breathing cycle is not the only intrafractional motion to consider, for example, in some tumors there is also a motion due to the beating of the heart. (Shirato et al., 2004). When preparing a treatment plan, in addition to the motion of the tumor volume itself, the movement of close critical organs and tissues of varying densities entering and exiting the path of the beam most be accounted for. Therefor a successful treatment of moving organs requires the assessment of these motions with volumetric imaging. The effect of the motions have to be accounted for, and compensation for, and/or reduction of, these motions has to be included when the patients treatment plan is made. (NuPECC, 2014) This accounting and compensation for intrafractional motion is what is refereed to as a 4D setup (Shirato et al., 2006).

To be able to account for the motion of the target, there is a need to image the three dimensional position of the target and how this position changes with time, so called 4D-imaging. Currently most imaging of organ motion is done with 4D-CT. This is a high exposure imaging technique which means that only a snapshot of the patients breathing cycle can be imaged. Because of this, the motion trajectories found with this technique can not be expected to represent the motion during treatment. But a CT-scan is needed to calculate the water-equivalent path length (WEPL). A possible solution for this is taking only a static CT for the WEPL and use a prolonged 4D-MRI-scan to investigate the motion. (NuPECC, 2014)

The use of markers is another widely used technique for detecting tumor motion and although effective, is also widely discussed. Since the markers are often very dense they can lead to range deviation from the dose plan if the marker move into the beam. This is especially a problem for the spot-scanning technique since it depends on its accuracy. (NuPECC, 2014)

The way markers are used is by placing them close to the target and imaging the patient, most often with CT, to obtain the coordinates of the marker. This is done over a time period of 1 to 2 minutes while measuring the position of the markers several times per second to obtain a motion map, or motion trajectories, of the target. With the aid this map the coordinates of the beam spots and when in the motion cycle the treatment should occur can be decided. To account for interfractional motion this procedure has to be redone before each new irradiation of the patient, this to ascertain how the motion map has been changed and compensate for it. (Shirato et al., 2006)

In Japan, this way of tracking the target volume has now been integrated into a

system that tracks the tumor in real-time during treatment with the use of a proton scanning beam. And it is reported that this system reduce irradiation volume by 50-75 percent when compared to conventional methods that irradiate the entire volume the target might move within during treatment. (Hitach, ltd, 2014)

This system has garnered attention because it is a step towards an ideal where the accuracy of particle therapy is combined with real-time (or online) measurement of the target position.

There are also several technique for reducing motion and reducing dose errors related to the interplay between the scanning motion and the tumor motion. An example of reducing motion is gating, where the beam is only delivered if the target is within a certain range or window. This leads to longer treatments due to the beam only being delivered during parts of the patients breathing cycle. (NuPECC, 2014)

For the interplay effect, so called repainting or rescanning can be used. The goal of this is to average out the errors that arise as a consequence of the beam and target moving simultaneously. This has the added benefit of averaging out any other errors that are variable with time. (NuPECC, 2014)

For spot-scanning, ideally the tumor motion would be imaged during treatment and the positioning of the spots changed in accordance with this image. Since this require the WEPL data and the dynamic change of the beam range, this can currently only be done with 4D-CT and a accelerator/beam delivery system that can quickly change the energy of the delivered beam. Current imaging research is investigating the possibility of theranostics or particle radiograpy/tomography, sometimes referred to as proton CT, as a low-dose alternative to CT. While this would be close to ideal the computational requirements for such treatments will be very high. (NuPECC, 2014)

When considering the interfractional motion, the uncertainties caused by the movements on this scale is reduced if the patient is imaged on the day of the treatments and the treatment plan is adjusted in accordance with these images. (Shirato et al., 2006) Interfractional motion can also be accounted for by placing a margin around the tumor, this is possible since interfractional motion mostly cause deviations from prescribed dose on the edges of the irradiated volume. (Lambert et al,, 2005)

The volume that has been identified as a tumor is defined as the Gross Tumor Volume (GTV). This volume is then extended to include the volume around the GTV where tumor involvement is suspected, this extended volume is called the Clinical Target Volume (CTV). At this point the margin previously mentioned is added to the CTV, forming the Planning Target Volume (PTV). The PTV is meant to account for uncertainties related to patient movement, differences in patient positioning (scanning positioning vs treatment positioning) and organ motion. The extending of the CTV into the PTV hopes to ensure that the CTV receives the planed dose. (Langen and Jones, 2001)

However, setting up a margin around the target dose decrease the dose conformity to the target which is one of the major advantages of particle therapy. (NuPECC, 2014)

Interfractional motion is most prominent in organs that are part of or, located close to, the digestive system. The displacement of the tumor volume often correlate with rectal or bladder movement. The state of the rectum, full vs empty, will for example, affect the position of the prostate. (Langen and Jones, 2001)

This correlation is also the reason rectal balloons are used in treatment of prostate

cancers to decrease the volume the prostate has available to move. Both this technique and abdominal compression, reduce available volume for motion. This has the effect of reducing the amplitude of the target motion. (NuPECC, 2014)

These correlations between the position of organs in the abdomen and bladder and rectal volume leads to treatment standards at some facilities to state that treatment should be done with the patient having a “comfortably full bladder” this due the correlation between bladder filling and the motion of the small bowel, and is done in an attempt to spare the small bowel from the treatment field when treating pelvic tumors. (Jadon et al., 2014)

An other cause of interfractional motion is the condition of the patient, such as a wight gain or loss which can also affect the position of the tumor volume. (Langen and Jones, 2001) It has also been shown that the bladder volume is systematically reduced during the course of the treatment (Jadon et al., 2014), meaning that the treatment itself can influence change in the patients internal geometry.

1.3 Monte Carlo Simulations

Monte Carlo simulations works by repeatedly calculating a possible physical interaction based on a probability distribution. When the number of repetitions become high enough, a good representation of a numerical solution of the problem can be achieved. This solution will then be dependent on the defined parameters of the simulation. When considering Monte Carlo simulations of radiation and/or particle interactions these parameters are the defined geometry, which is most often defined by the user, and the cross sections of the relevant interactions, often given by the different programs with the option of user defined changes to cross section and/or the selection of which interactions are relevant to the simulation.

Monte Carlo simulations are a valuable tool to theoretically predict outcome of experiments but do require a high amount of computational power or, alternatively, time for the calculations. This means that traditionally Monte Carlo simulations have mostly been considered a research tool.

Since Monte Carlo simulations are tied so tightly to research and experiments most programs will be regularly updated with the newest interaction cross sections and simulations will be done to compare the results obtained with actual experiments. Therefor Monte Carlo simulations can be considered to be fairly accurate excluding user mistakes. (Ytre-Hauge, 2013)

2 Method

The results where obtained by the use of the Geant4 and analyzed with ROOT.

2.1 Geant4

Geant4 is a free software package that contains tools that can applied for accurate simulations of particles passing through matter. It is written in C++ and uses advanced software-engineering and object-orientation for the sake of transparency.

While the initial purpose of Geant4 was to create a detector simulation program that could be applied to the next generation of sub atomic experiments. But as it became clear that the program had potential to be of benefit to communities such as nuclear, accelerator and space physics. And also, crucially for this work, medical physics. The scope of the project widened with the inclusion of individuals from these communities. (introduction to geant4)

My simulations where preformed with Geant4 version 10.0 patch-02 and with the QGSP_BERT_HP physics list. The reason for this particular physics list was that it was the recommended physics list for low energy dosimetry applications and Medical neutron applications. It also seemed to be an extension to one of two standard physics lists to include thermal neutrons. (Physics lists)

2.2 Geometry

The geometry of the application was built fairly simply. Inside the space that was used for the simulation there had been placed a 30x30x30 cm water phantom. And inside this phantom there was a 20x20x4 mm water target that had been linked to a custom scorer. The scorer measures the energy deposition and x and y position of the particles that hits the target and was based on an example in one of exercise from the second geant4 international school.

The target is placed with the center of the target 1 mm away from the center of the phantom, towards the beam. This means that the beam enters the target after traveling through 14,7 cm of water and exits the target after 15,1 cm. This placement is a remnant of the earlier versions of the program and was not discovered before simulations was well on their way. This placement should not influence the results as the beam energy is tailored to place the Bragg peak in the center of the target. One parameter that can affect the results to a degree is the somewhat small layer thickness of 4 mm. This means that the some of the energy gets deposited in front of and behind the target. See figure 2.2.1.

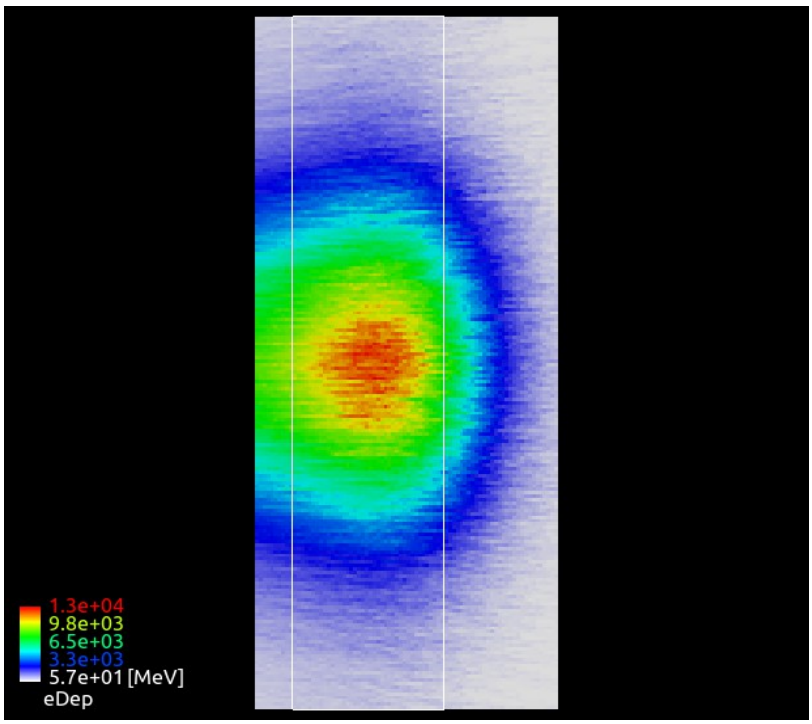

Figure 2.2.1: The figure shows the energy deposition in the yz-plane of a beam spot of 100000 protons. The white outline is the target.

2.3 Beam

The beam is a circular proton beam with a radius of 2 mm. The beam starts 16 cm from the center of the phantom and travels through 1 cm of geant4 “vacuum” before entering the phantom. The beam energy is 145,60 MeV, gauss distributed with a 0,1456 MeV standard deviation. The figure below is a plot of the beams distribution of particles in the x-direction for one beam spot of 100000 protons and show that, when the beam hits the target it has a full width half maximum of around 8 mm.

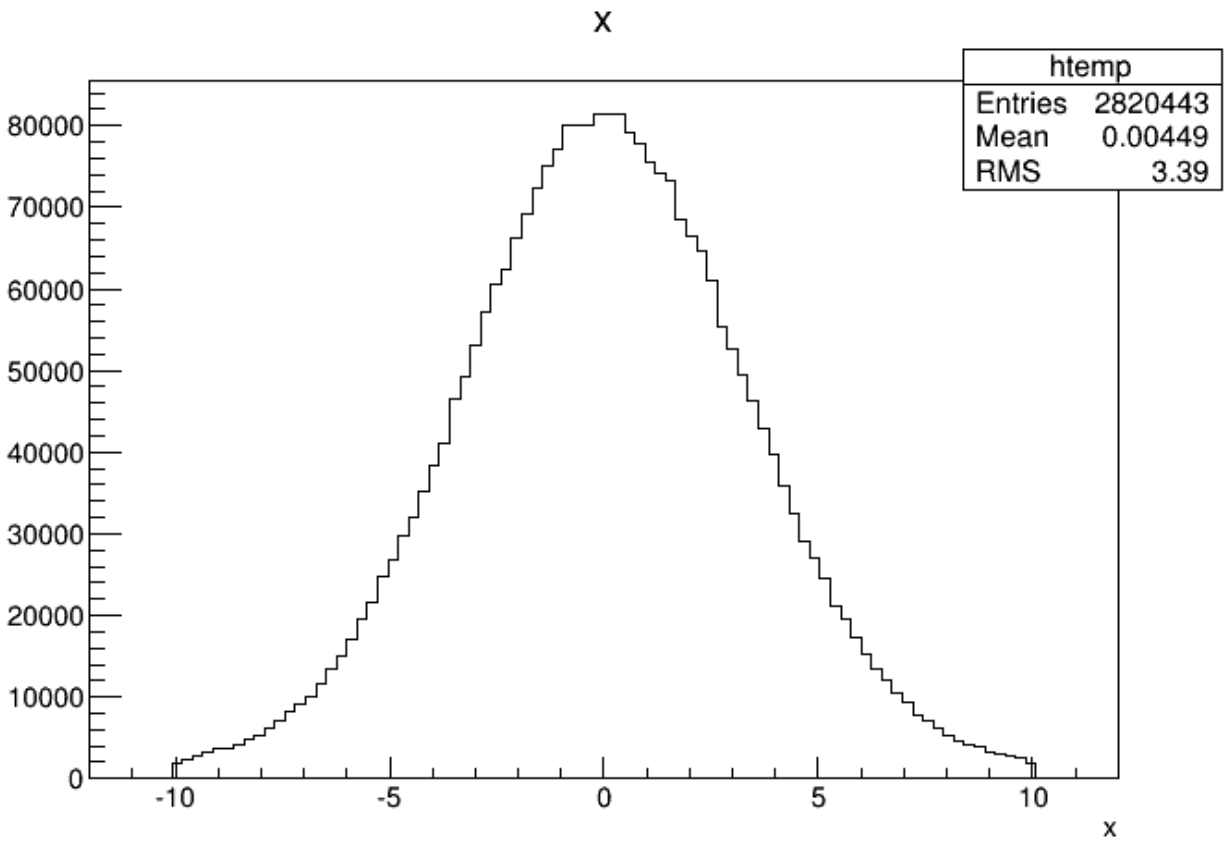

Figure 2.3.1: Distribution of the energy depositions in the x-direction in mm of a 100000 proton beam spot. The full width half maximum is approximately 8 mm.

The scanning of the beam over the target is simulated by moving the source of the beam in the x and y direction. There is 25 beam spots in total that follows this pattern of movement.

$$x = 9 \text{ mm} \rightarrow x = 4{,}5 \text{ mm} \rightarrow x = 0 \rightarrow x = -4{,}5 \text{ mm} \rightarrow x = -9 \text{ mm}$$

While holding the y value constant at 9 mm, when the x value reaches the end of the pattern the y value is changed one step of the same pattern before the x pattern resumes, this time from negative to positive. The pattern then repeats, see illustration below.

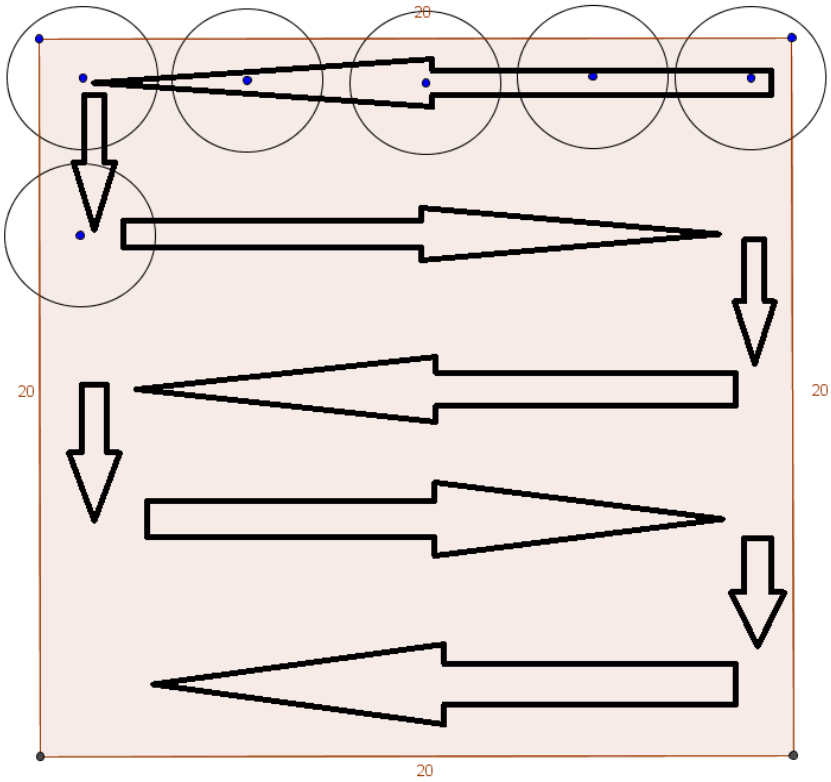

Figure 2.3.2: This illustration shows the positioning of the beam spots for scanning over the target.

When doing the repainting simulations the pattern was reversed for all even number scans (2, 4, 6, 8, 10) with the exception of one simulation set where the beam position was reset to 9 mm x and 9 mm y and followed the scanning pattern from there for every re-scan. This for the purpose of comparing these two different ways of repainting.

2.4 Movement

The movement of the target was simulated by changing the position of the target when the beam spot was moved. This means that the target was only moved in stages. For the basic simulations the author assumes a displacement of the target to be 1 cm per sec in all directions included in that particular simulation. This assumption is based on average magnitude of motion from the periodic breathing cycle produced by Mohn and Wasbø, see figure.

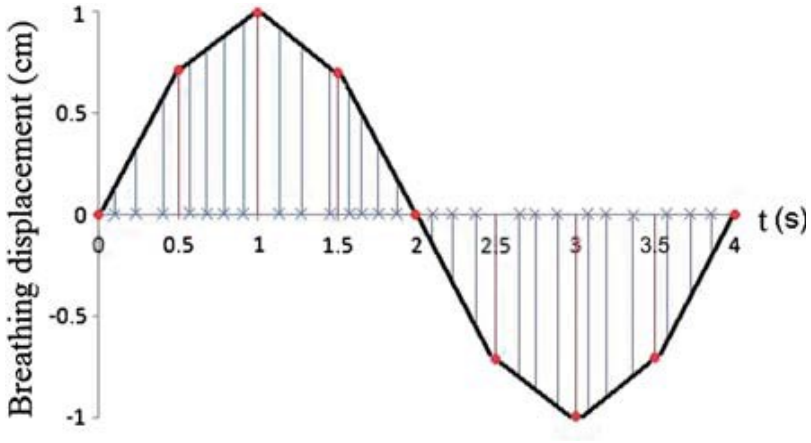

Figure 2.4.1: A breathing cycle as a periodic function. Illustration from Mohn and Wasbø.

And the length of the spill to be 1 sec. This means that for 25 beam spots (no repainting) every time the beam spot was moved, the target was moved 0,4 mm in the direction that particular simulation called for. This means there is a time scale of 0,04 sec per beam spot, which is quite large. For the repainting simulations there was 250 beam spots within the same time frame, meaning the target was moved 0,04 mm for every movement of the beam. The time per beam spot would then be 0,004 sec or 4 ms which is within typical beam spot irradiation times (Yupeng et al. 2014).

For the gating simulations breathing cycle of Mohn and Wasbø was followed more closely and the interval from 0,5 sec to 1,5 sec in the breathing cycle was used. From 0,5 to 1 sec the target is moved half of what it would be moved without gating, 0,2 mm for no repainting and 0,02 mm for repainting. From 1 to 1,5 sec the magnitude of the movement remains the same but the direction is reversed.

For the “Full treatment” simulation the entire breathing cycle was used and extended to encompass 10 scans with a 0,5 sec pause between re-scans. These scans was applied as repainting, meaning that the odd number scans started in a positive beam spot and even the even numbered scans in a negative beam spot. To simplify the displacement of the target, the target was only displaced 0,6 mm or 0,2 mm between beam spots. This leads to a slight difference from the breathing cycle as the

movement of the target will be slightly larger when the displacement is nearing 0,75 cm from 0 cm and a slightly smaller movement when the target is nearing 0,75 cm displacement from 1 cm.

The ICRU recommend that scanning techniques should not be used for targets with motion amplitudes of 10mm or greater. (Kraus et.al, 2011, see further references therein.) With the exception of the simulation of the gating window these simulations are at the very limit of this recommendation and we should therefor expect poor coverage of CTV that will be defined from the static simulation.

2.5 Simulations

In all the simulations a total of 25 million protons was used, meaning for no repainting there was 1 million protons per beam spot and for repainting and re-scanning there was one hundred thousand protons per beam spot. When the particles hits the target the depositions of energy gets registered and written to a csv-file. The data gathered consist of the x and y positioning of the deposition in millimeters and the deposited energy in keV.

The simulations that was preformed was as follows:
No repainting: no movement, movement in the positive and negative x directions, movement in the positive and negative y directions, movement towards the beam, movement in the positive x direction and the positive y direction, and movement in the positive x and negative y direction simultaneously.

Repainting: Movement in the positive x direction with and without alternating scanning direction, Movement in the positive and negative y direction, movement in the positive x and y directions.

Gating: Movement starting in the positive x direction with and without repainting, Movement starting in the positive y direction, movement starting in the negative y direction, and movement starting in the positive x and y directions with and without repainting.

Full treatment: Movement of the target in the x direction, following the breathing cycle produced by Mohn and Wasbø

3 Results

In this chapter the results from the Monte Carlo simulations are presented. The simulation data was stored in the csv formate and filled into a ROOT two-dimensional histogram with the energy as the weighting of each xy position. This means that the total energy deposited in the plot is the integral of the entires. The histograms have a range from -12.5 mm to 12.5 mm in both x and y directions and 125 bins in both the x and y directions. This was done to make sure the histogram includes bins with zero energy deposition, and to make sure that any points outside of the -10 mm to 10 mm range of the target (that should not exist) gets discoverer.

3.1 Static

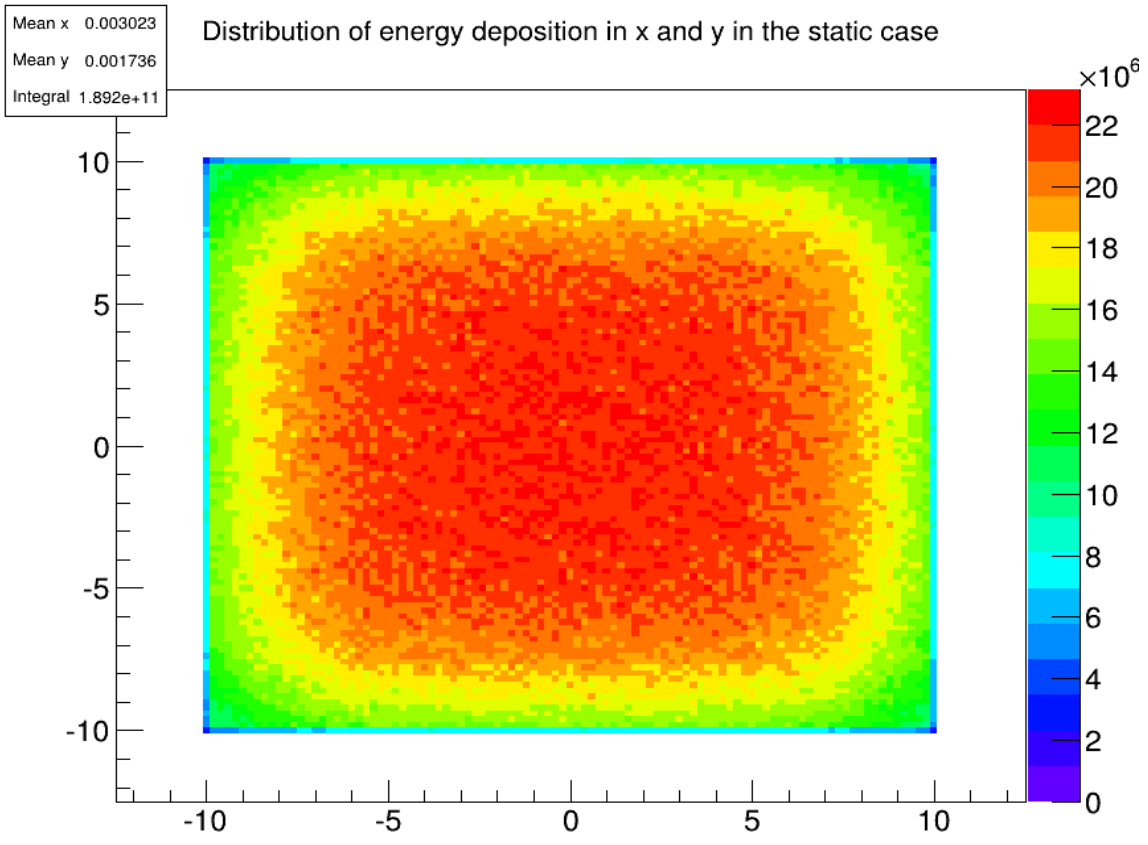

Figure 3.1.1: Plot of the energy deposition in x and y with no movement of the detector.

The first plot is the static case. This will be used as the basis for comparison in the plots of the moving targets. As can be seen from figure 3.1.1 above, the energy deposition does not form a perfect square as the edges are rounded. Because of this an investigation of x and y slices of the plot was made, and the ranges -6.5 mm to 6.5 mm for the x and y axis was set to be the CTV. This was based on the approximation that the most common bin value in the red area was $21.5*10^6$ keV. This was then set as the ”prescribed dose” and the range where 90% of the “prescribed dose” was approximated.

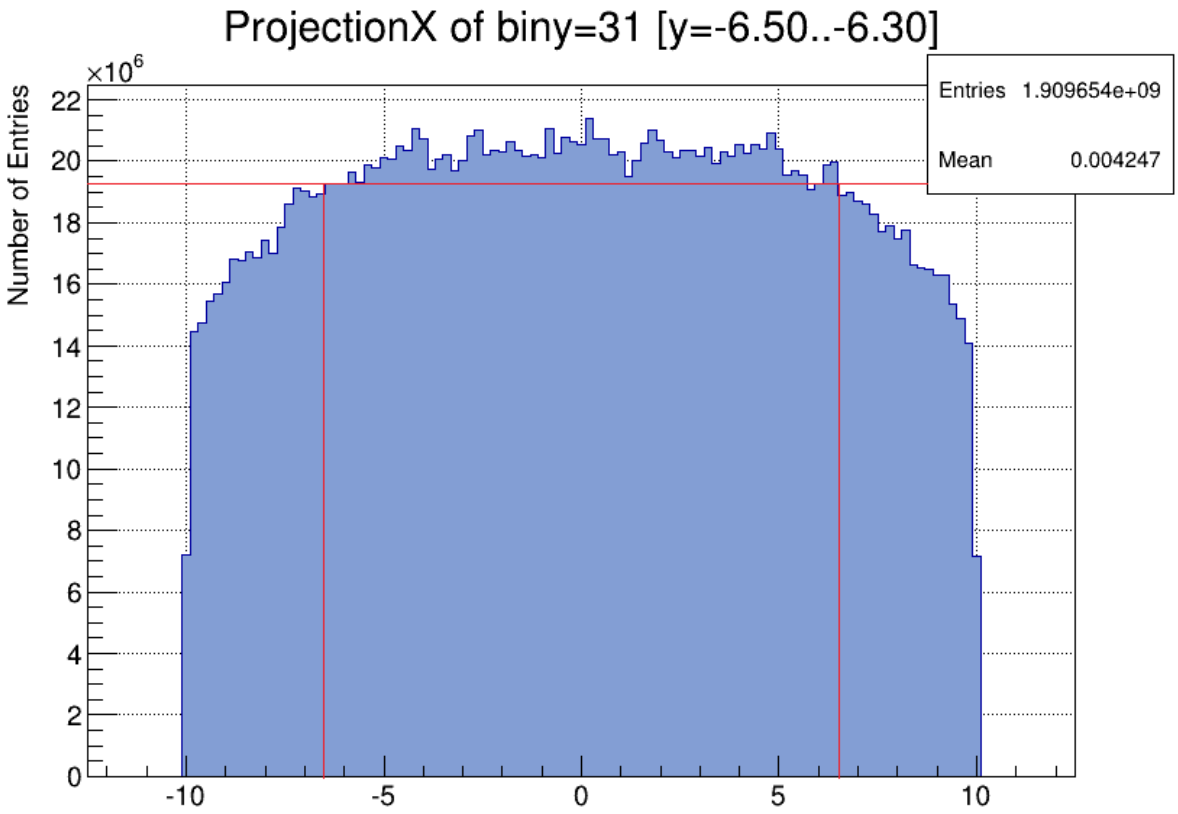

Figure 3.1.2: An x projection of the x values in the range -6.5 to -6.3 mm y. The lines represent an approximated 90% minimum threshold and show that 90% of “prescribed dose” is not achieved outside of the range -6.5 to 6.5 mm x.

In the movement plots a comparison between the plot in question and the static plot will be made of, the total deposited energy and, how much of CTV in the plot that has received 90% of “prescribed dose” or 21.5 GeV per bin.

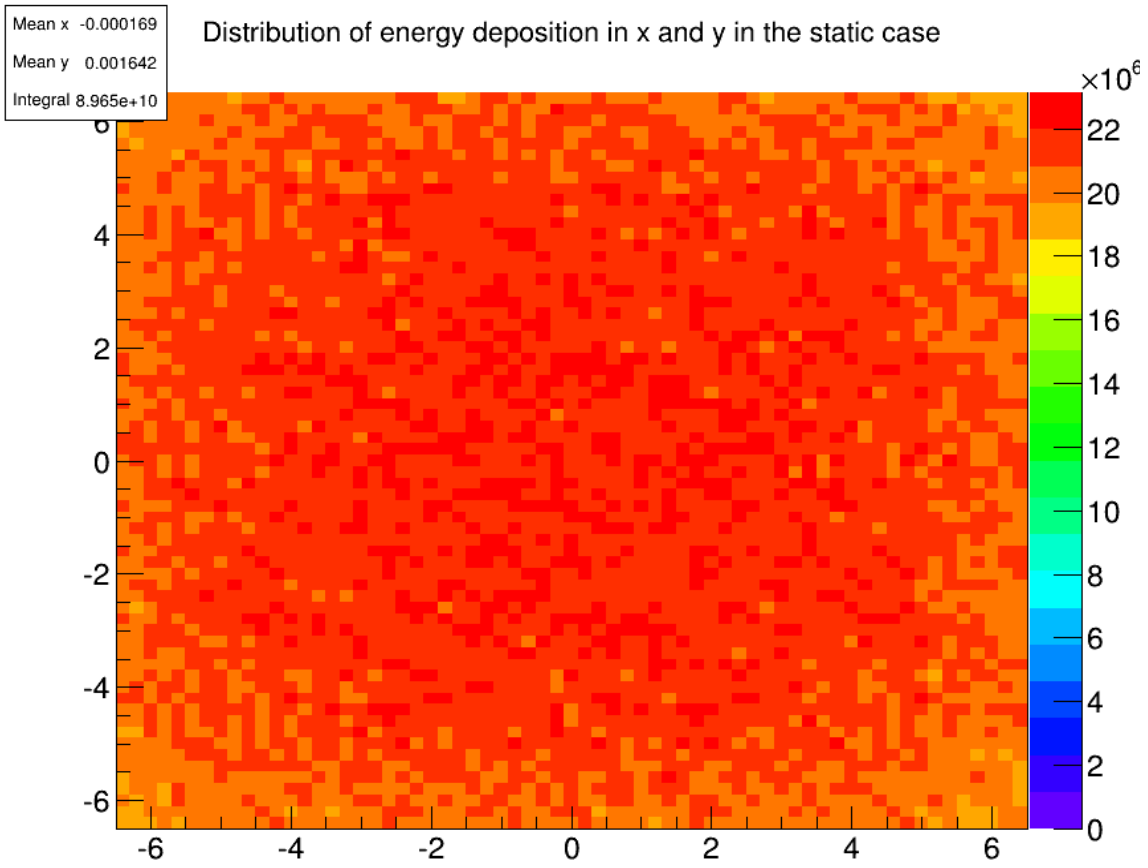

Figure 3.1.3: The distribution of energy deposition in x and y for the static simulation with the range set to show bins from -6.5 to 6.5 mm x and y.

In Figure 3.1.3 above representing the cut of the static plot, the majority of the bins are red, representing that xy positions where between, just under, 21 GeV and 22 GeV was deposited. There are also quite a few dark red representing above 22 GeV up to 23 GeV and dark orange representing around 20 GeV. All of which are withing ±10% of the prescribed dose. The orange bins will most often be outside the 10% of prescribed dose window.

3.2 X- movement

This chapter will present the plots from the simulations including only a target movement in the x direction.

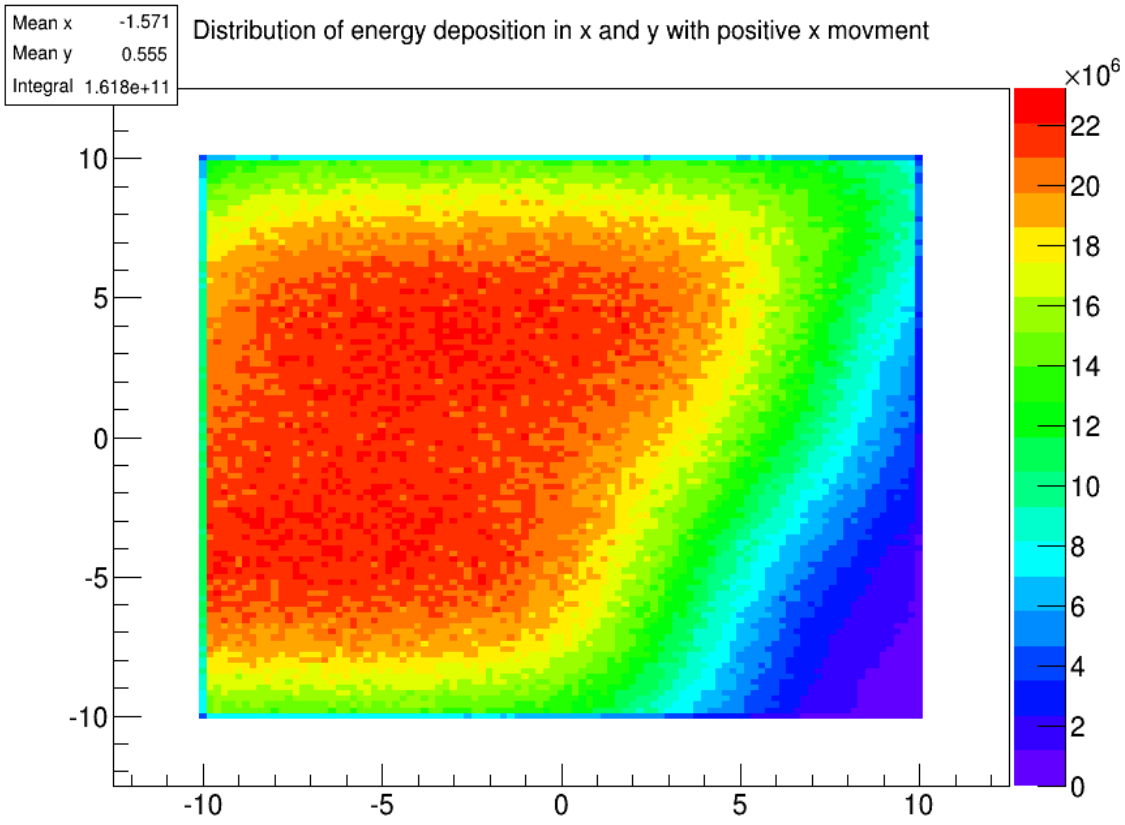

Figure 3.2.1: The distribution of energy deposition in x and y for the positive x movement simulation.

In this plot we can see how the positive x movement looks like a negative movement to the beam as the positioning of the beam spots become more and more negative on the target. Our central square of deposition gains a rhombus shape due to this gradual increase in the beam spot displacement. In the range from -6.5 mm to 6.5 mm (Figure 3.2.2) we see that about 89.6% of the total energy that was delivered in the static case was delivered to the moving target. We can also approximate from the plot that 32% of the CTV received less then 90% of the “prescribed dose”, or that only 68% of the target received 90% or more of the “prescribed dose”.

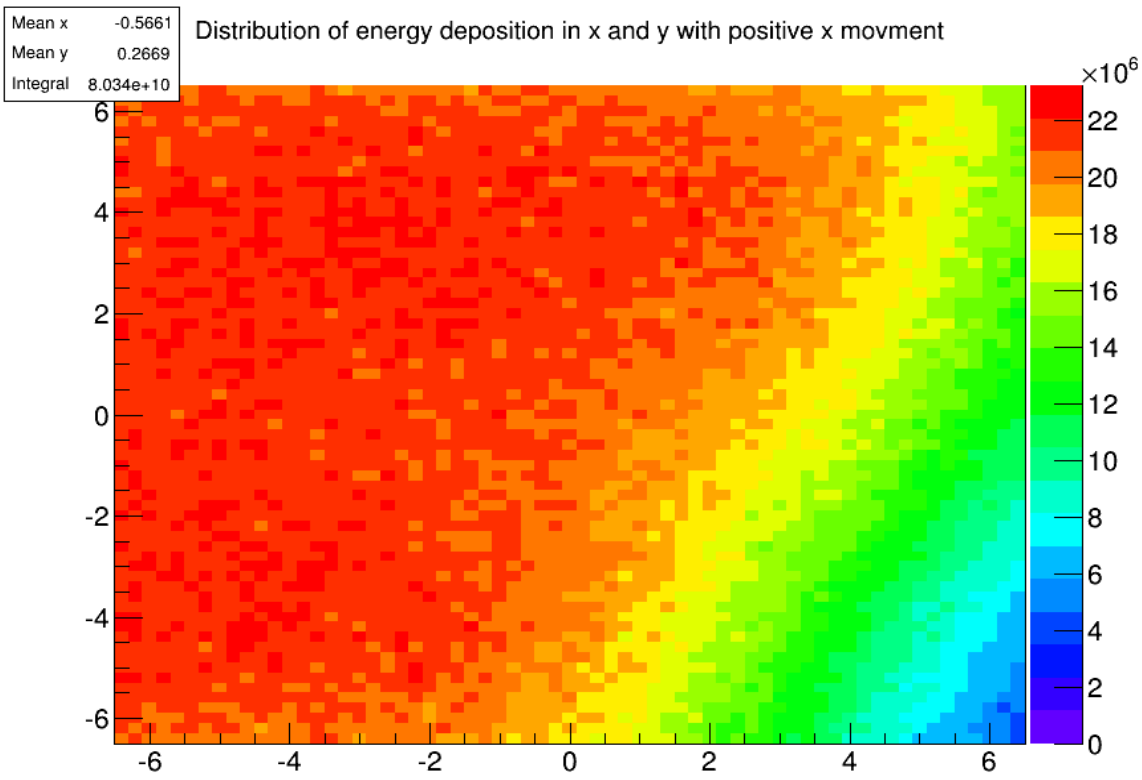

Figure 3.2.2: The distribution of energy deposition in x and y for the positive x movement simulation, with the range set to show bins from -6.5 to 6.5 mm x and y.

When the target moves in the negative x direction we get an almost identical plot with the exception that the beam spots have been displaced in the positive x direction. It could also seem like less of positive side of the rhombus disappears outside of the detector than the negative side of the positive x movement plot. This is supported by the difference in the total energy deposition between them. This difference could have come about because the scanning pattern moves in the negative x direction more often than in the positive direction, but the difference is small enough that the possibility that it is an statistical effect should not be discounted.

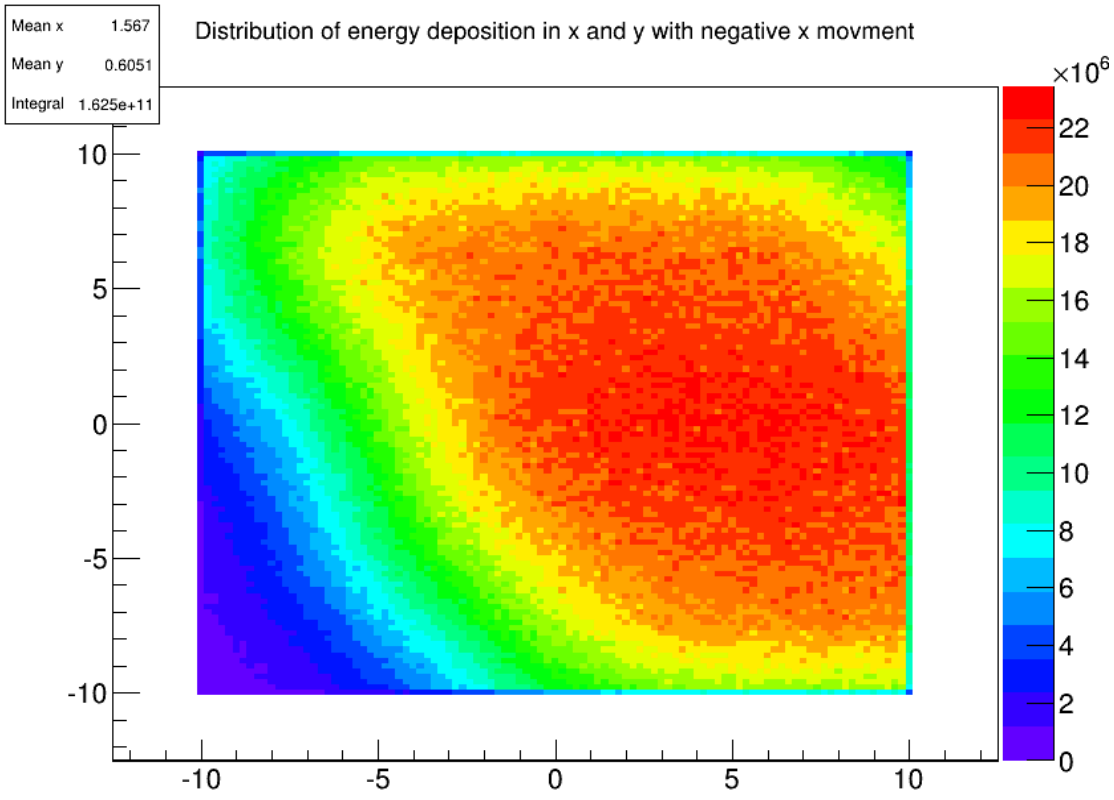

Figure 3.2.3: The distribution of energy deposition in x and y for the negative x movement simulation.

The CTV receives 89.4% of the total energy that was delivered to the CTV in the static case, and approximately 32% of the CTV received less then 90% of the "prescribed dose" when the target was moved in the negative x direction. This is also as expected, quite consistent with data from the positive x direction.

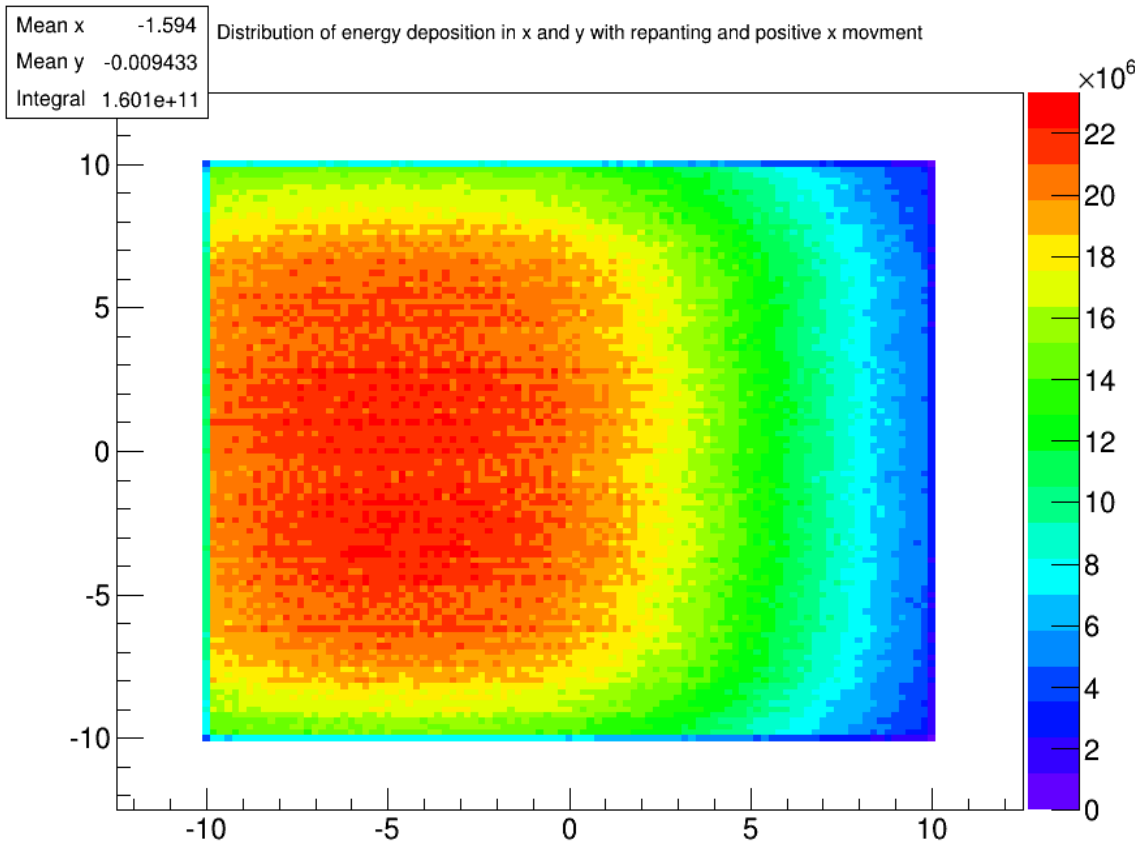

Figure 3.2.4: The distribution of energy deposition in x and y for the positive x movement simulation with repainting.

For the repaint simulation of positive x movement we can see that the square shape of the high dose area is maintained. Repainting can therefor be said to maintain the shape of a dose distribution, but does not seem to have any effect on displacement of the dose.

In fact the CTV only receives 87.5% of the intended energy, and approximately 38.5% of the CTV receives less than 90% of the “prescribed dose”. This is a poorer result than without repainting, though some of this can likely be linked to the big difference in step size in the two modes of simulation.

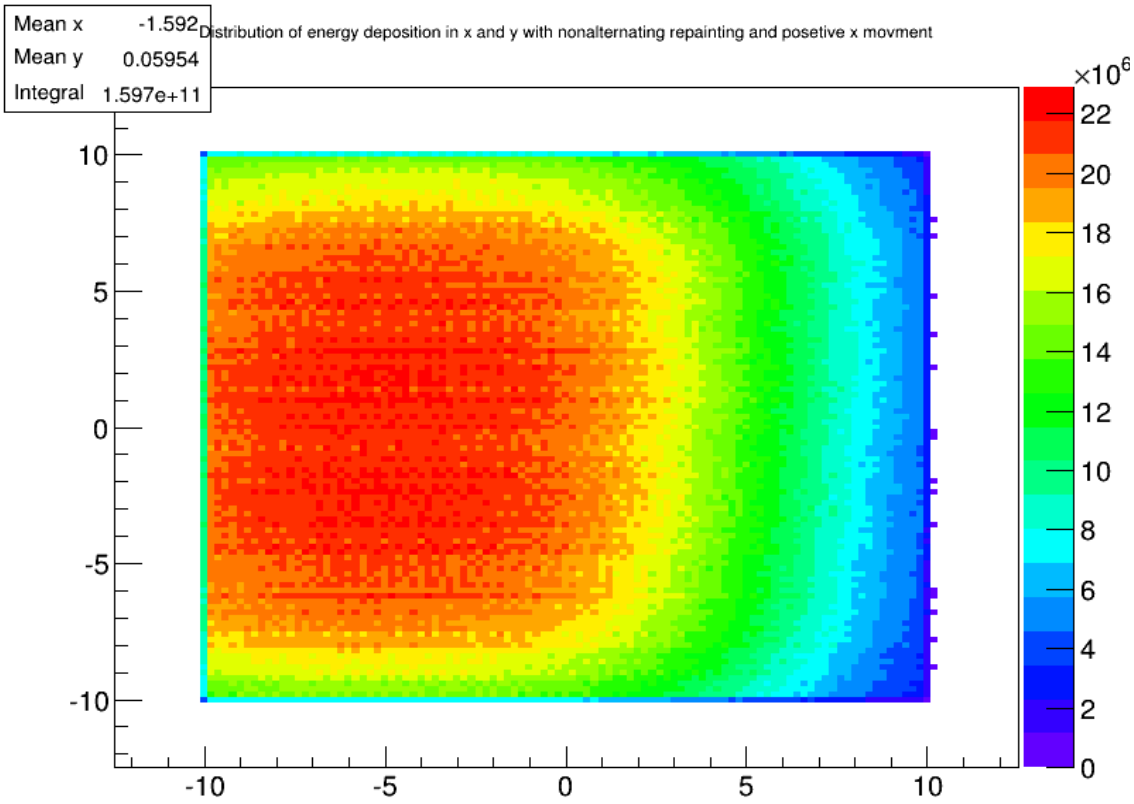

Figure 3.2.5: The distribution of energy deposition in x and y for the positive x movement simulation with non-alternating repainting.

When the repainting is done by reseting the beam position to the first beam spot, the distribution dose change slightly from the distribution with the alternating scanning directions. We can see that the high dose area regains a slight tilt, going back towards a rhombus shape. The reason behind this effect is that, by resetting the scanning pattern the positive y beam spots will always be less displaced than the negative y beam spots.

This tilt would then seem like the reason behind the slightly better coverage of the CTV with approximately 37% of the area receiving less than 90% of the “prescribed dose”. The total energy deposited is slightly down however with it being 87% of the static case.

3.3 Y-movement

This chapter will present the plots from the simulations including only a target movement in the y direction.

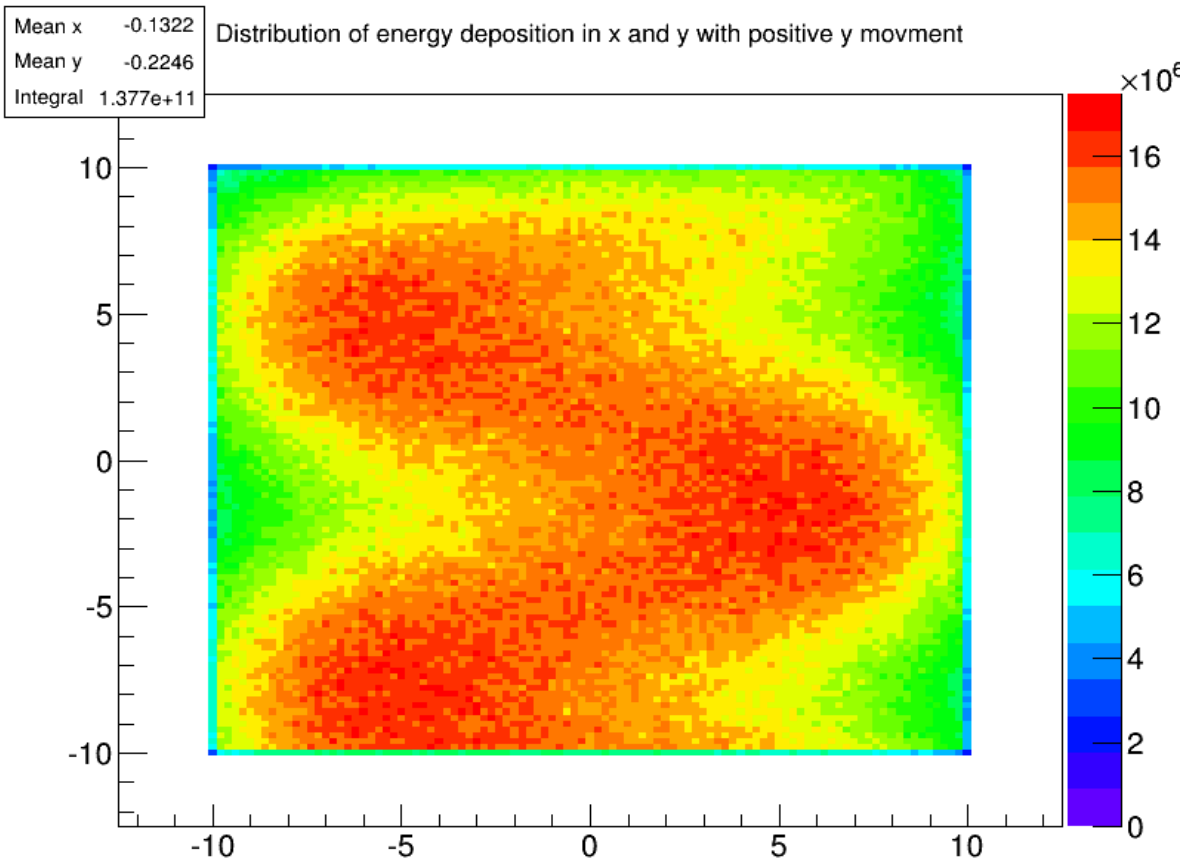

Figure 3.3.1: The distribution of energy deposition in x and y for the positive y movement simulation. Note that the color scale only goes to approximately 17 GeV.

When the target moves in the positive y direction the distribution ends up being stretched out as the beam scans down the negative y direction, forming a zig-zag pattern. The amount of energy getting deposited outside the target area is also large, with 27.2% of the energy deposited in the static case now being deposited outside the detector. Together this leads to the distribution not reaching 90% of "prescribed dose" at any point in the CTV, and even though the CTV is located in one of the regions of higher dose it only receives 70.3% of the energy deposited in the static case.

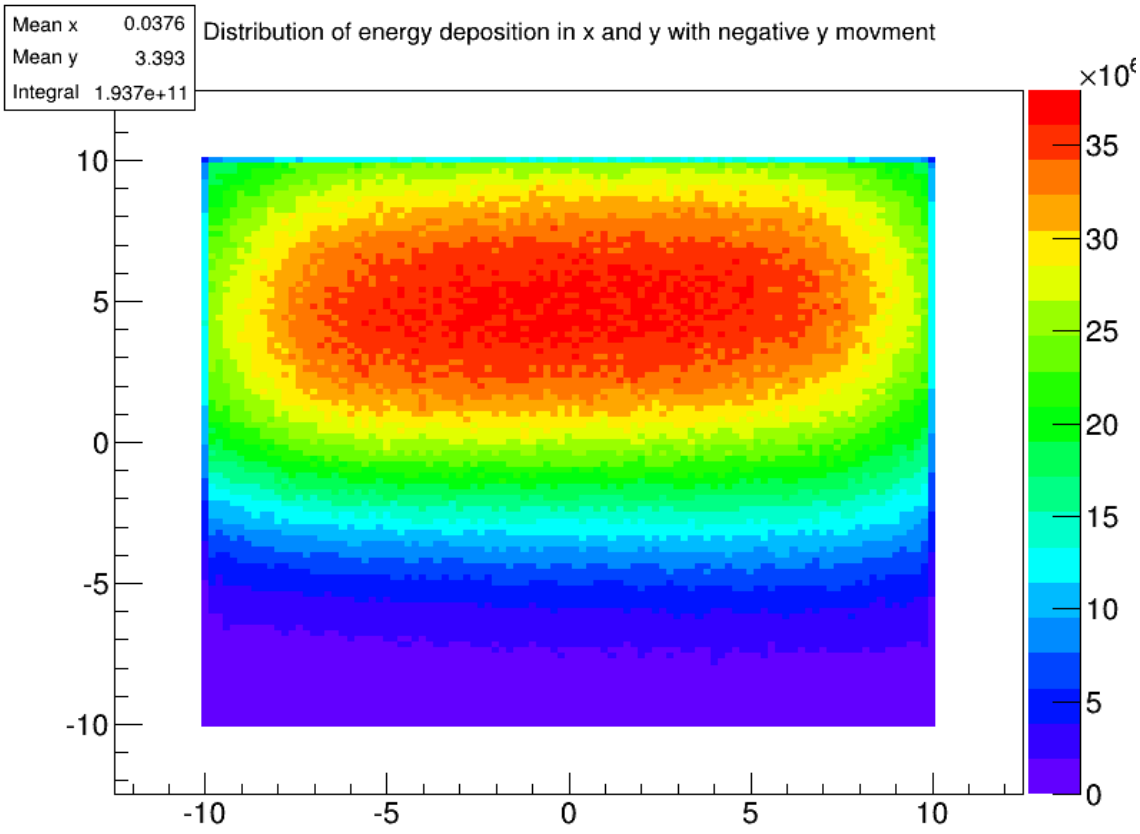

Figure 3.3.2: The distribution of energy deposition in x and y for the negative y movement simulation. Note that the color scale goes to approximately 38 GeV.

In the case of negative y movement the situation is reversed. Here instead of the distribution being stretched out it gets compressed by way of the beam spots in the negative y being displaced towards positive y, as a consequence the shape of the high dose area is changed from square to oval. The compression also leads to a higher total energy deposit, about 2.4% more, when compared to the static case, this because the beam spots in the negative y range will deliver less energy outside the detector.

This leads to over dosing, over 110% of "prescribed dose", in approximately 54% of the CTV and under dosing, under 90% of "prescribed dose", in approximately 38% of the CTV. All told there is deposited 8.3% more energy in the CTV in the negative y movement simulation than in the static case.

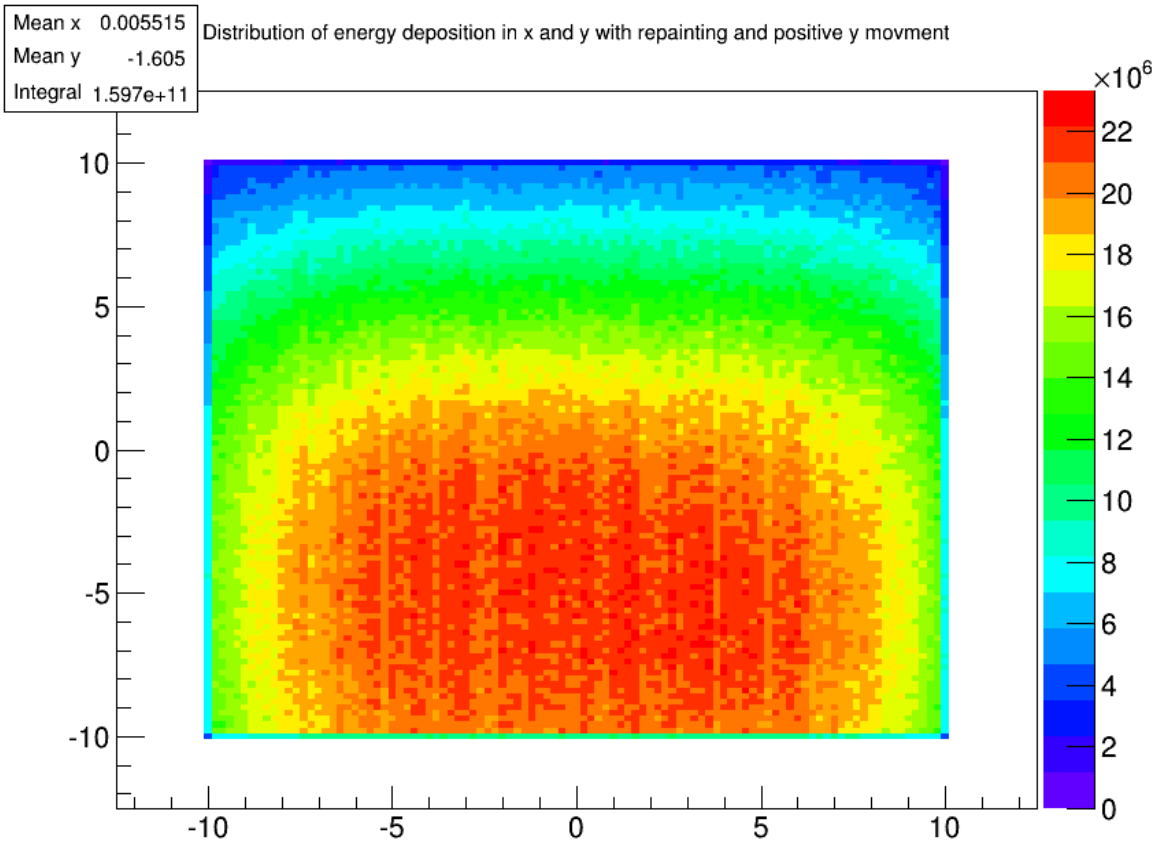

Figure 3.3.3: The distribution of energy deposition in x and y for the positive y movement simulation with repainting.

For the positive y movement repainting has a much greater impact than it did in the x direction. The stretching out of the distribution disappears and is replaced by a simple displacement of the high dose area like in the x direction case. The square shape is also back and there is a marked increase in the total energy deposited in the detector compared to no repainting.

The energy deposited in the CTV is also quite comparable with the repaint in the x direction. With approximately 38% of the CTV receiving less than 90% of the "prescribed dose" and the total energy deposited in the CTV being 86.9% of the static case.

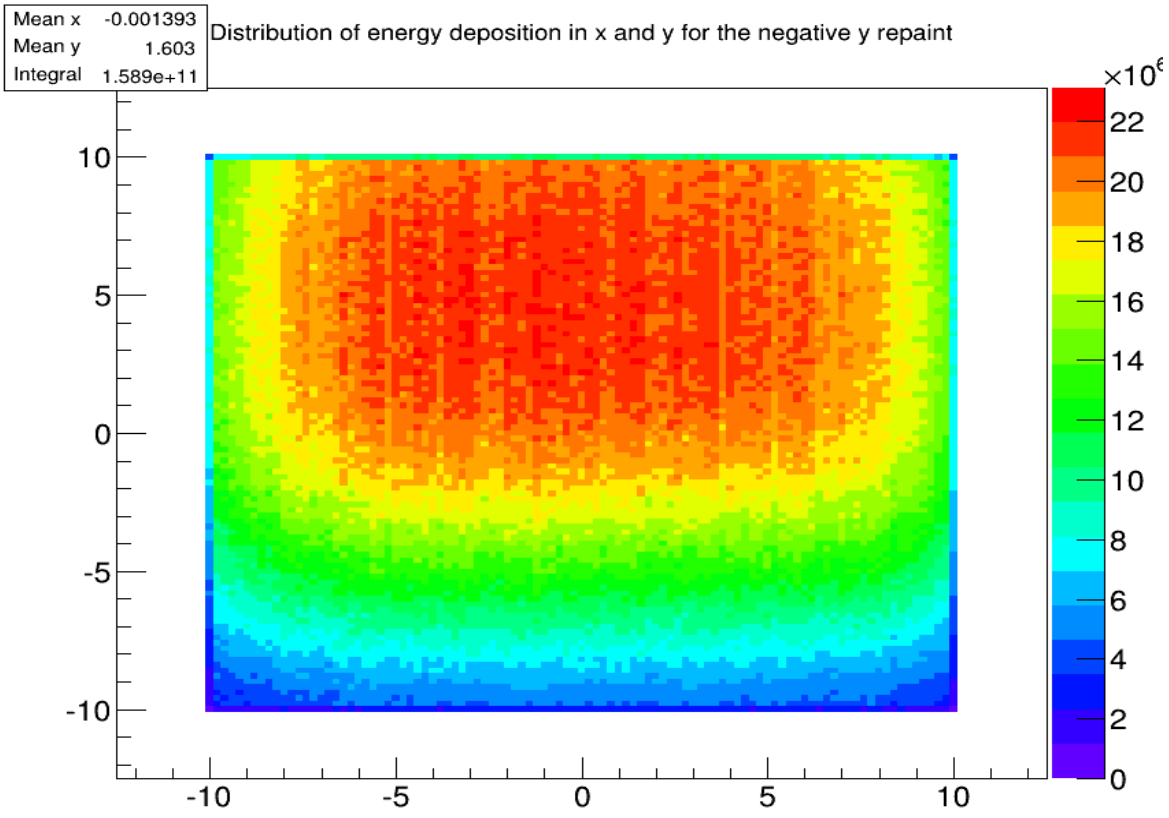

Figure 3.3.4: The distribution of energy deposition in x and y for the negative y movement simulation with repainting.

The same can be seen with the negative y movement repainting. The compression of the distribution is loosened and becomes quite similar to the distribution for the positive y repainting or indeed the x repainting. In the negative y movement repainting, CTV received 86.4% of the the energy deposited in the static case while approximately 40% of the CTV received less then 90% of "prescribed dose". Which again is quite comparable to the other repainting simulations. Though it seems that slightly more of the energy gets lost outside the target than with the positive y movement counterpart.

3.4 Z-movement

This chapter will present the plot from the simulation including only a target movement in the z direction.

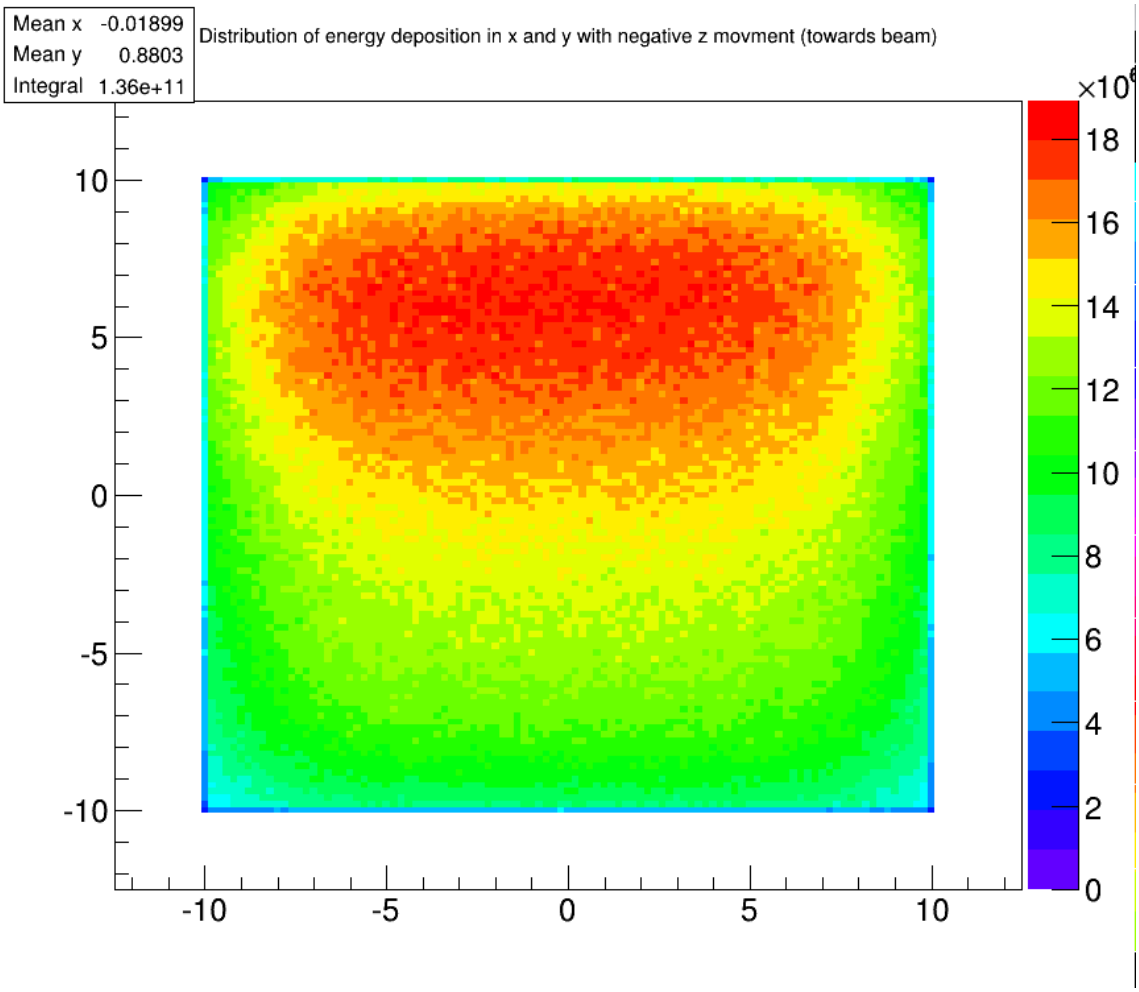

Figure 3.4.1: The distribution of energy deposition in x and y for the negative z movement simulation. Note that the color scale only goes to approximately 19 GeV.

In this plot we can see a fading out of the dose. With the first line of beam spots depositing energy close to the static case and then the beam depositing less and less as the target moves into the beam and therefor places the Bragg peak outside of the detector. In total the detector registers 71.9% of the energy registered in the static case. Since much of the beams Bragg peak is outside the detector when the beam spots reach the CTV this plot, like the plot showing the energy distribution when the

target moves in the positive y direction, will also not reach the minimum of 90% of the “prescribed dose”. In total the CTV receives 70.2% of the energy deposited in the static case.

3.5 XY-movement

This chapter will present the plots from the simulations including a target movement in both the x and y directions.

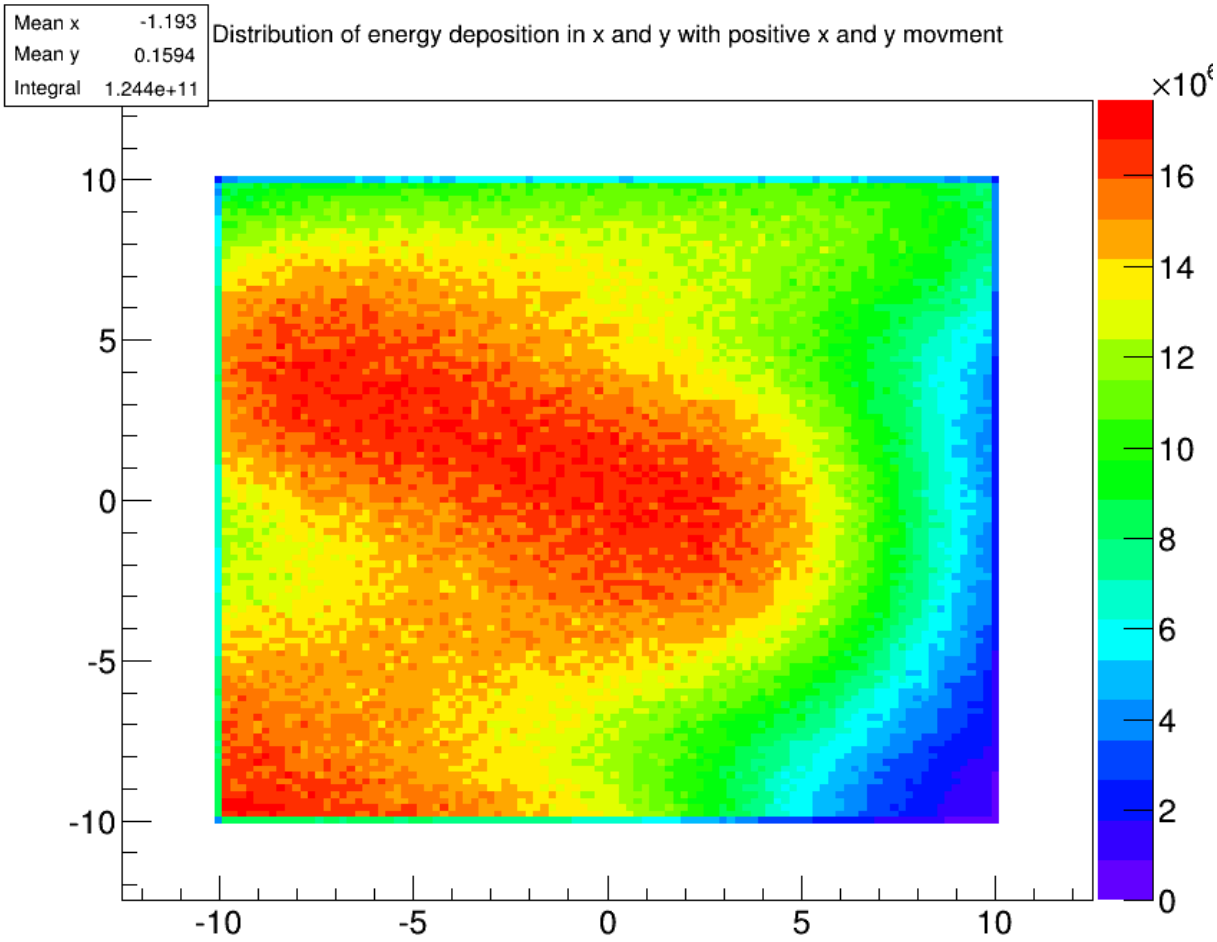

Figure 3.5.1: The distribution of energy deposition in x and y for the positive x and y movement simulation. Note that the color scale only goes to approximately 18 GeV.

As seen from the plot the effect of moving the target in both the x and y direction is that the separate x and y displacements gets added to each other, but while the shape is recognizable as a x displaced version of the positive y plot, it dose have some differences. When positive y movement is introduced the square of the static case gets stretched into a zig-zag pattern but with the inclusion of positive x movement the upper part of the pattern gets more gathered and the lower part of the pattern is displaced further away. In total the detector registers about 66% of the energy deposited in the static case and despite the slight increase of max bin energy in the CTV because of the x movement, the CTV still dose not achieve a minimum of 90% of the "prescribed dose". The total deposited energy in the CTV is 68% of the energy deposited in the static CTV.

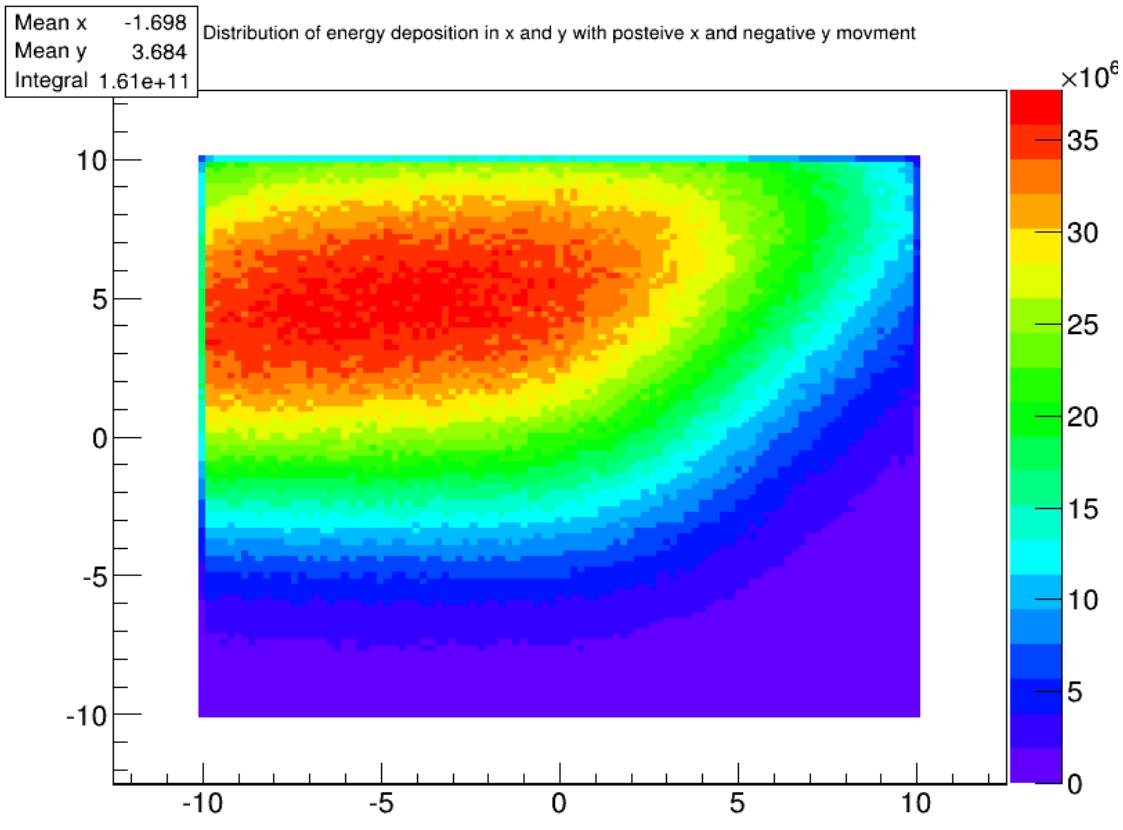

Figure 3.5.2: The distribution of energy deposition in x and y for the positive x and negative y movement simulation. Note that the color scale goes to approximately 38 GeV.

When the negative y and positive x directions are simulated together it results in the almost oval shape of the negative y distribution to change into a parallelogram due to the displacement of the negative y beam spots towards negative x. This leads to more of the energy leaving the area of the detector. In total the energy registered is 85% of the energy registered in static simulation. The total energy deposit then have more in common with positive x movement simulations then the negative y movement simulation. This is hardly surprising since the negative y movement didn't change the total energy deposition much, rather it concentrates it in the positive y part of the target. It is however a lower total energy than the x plot, this is likely due to the positive y beam spots depositing more of their energy outside the detector than in the simulation with only x movement.

In the CTV approximately 37% of the area receives a dose higher than 110% of the “prescribed dose” and approximately 49% of the area receives a dose lower than 90% of the “prescribed dose”. The total energy delivered to the CTV is 90% of the energy deposited in the static simulation.

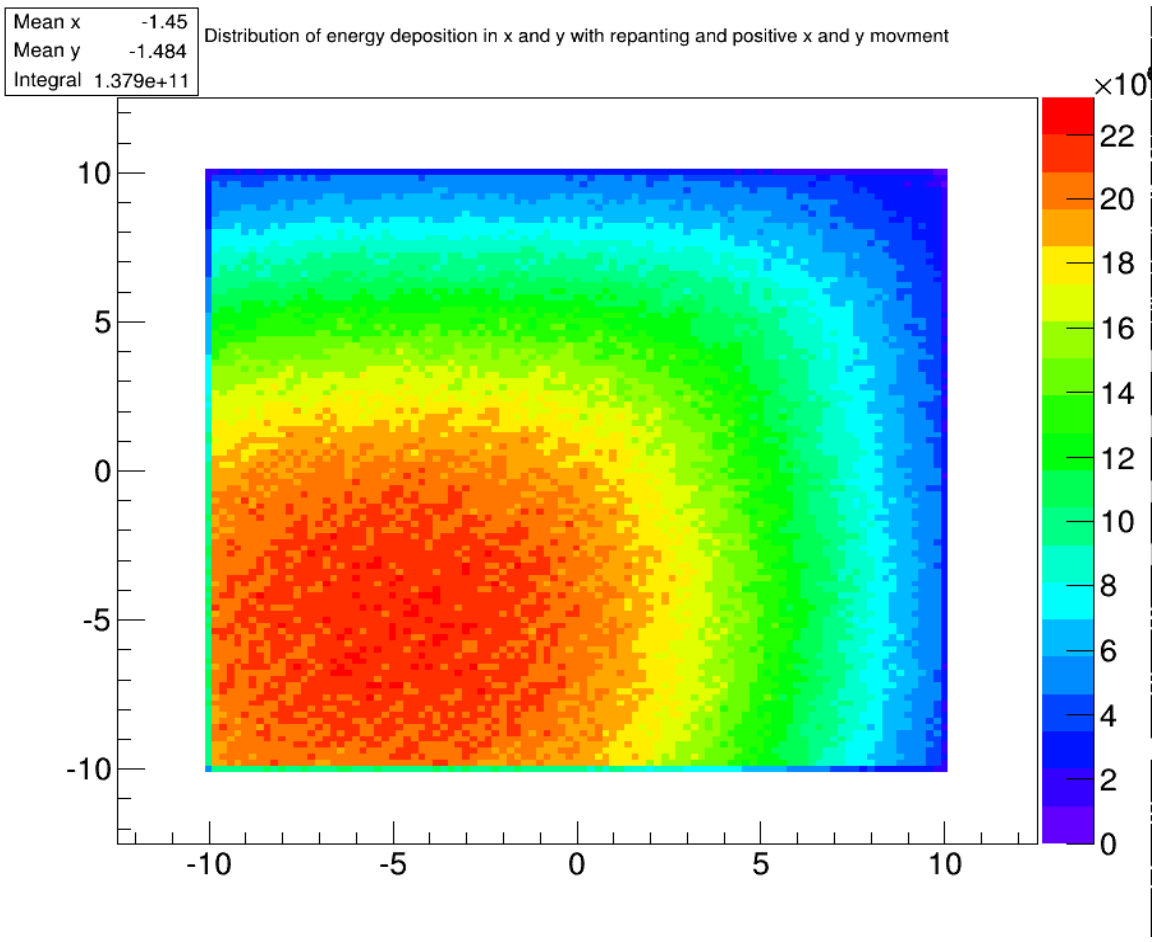

Figure 3.5.3: The distribution of energy deposition in x and y for the positive x and y movement repaint simulation.

Like in the previous repaint simulations the stretching out effect from the positive y movement is gone and so is the tilting effect of the positive x movement. This leaves us with a square shaped high dose area that has been displaced towards negative x and y. The detector registers 73% of the energy that was deposited in the static simulation. A marked increase compared to the no repaint plot of the same movement.

In the CTV, approximately 33% of the area receives a minimum dose of 90% of the "prescribed dose", and 77% of the total dose delivered in the static simulation is delivered in this case.

3.6 Gating

This chapter will present the plots from the simulations including a target movement in the gating window.

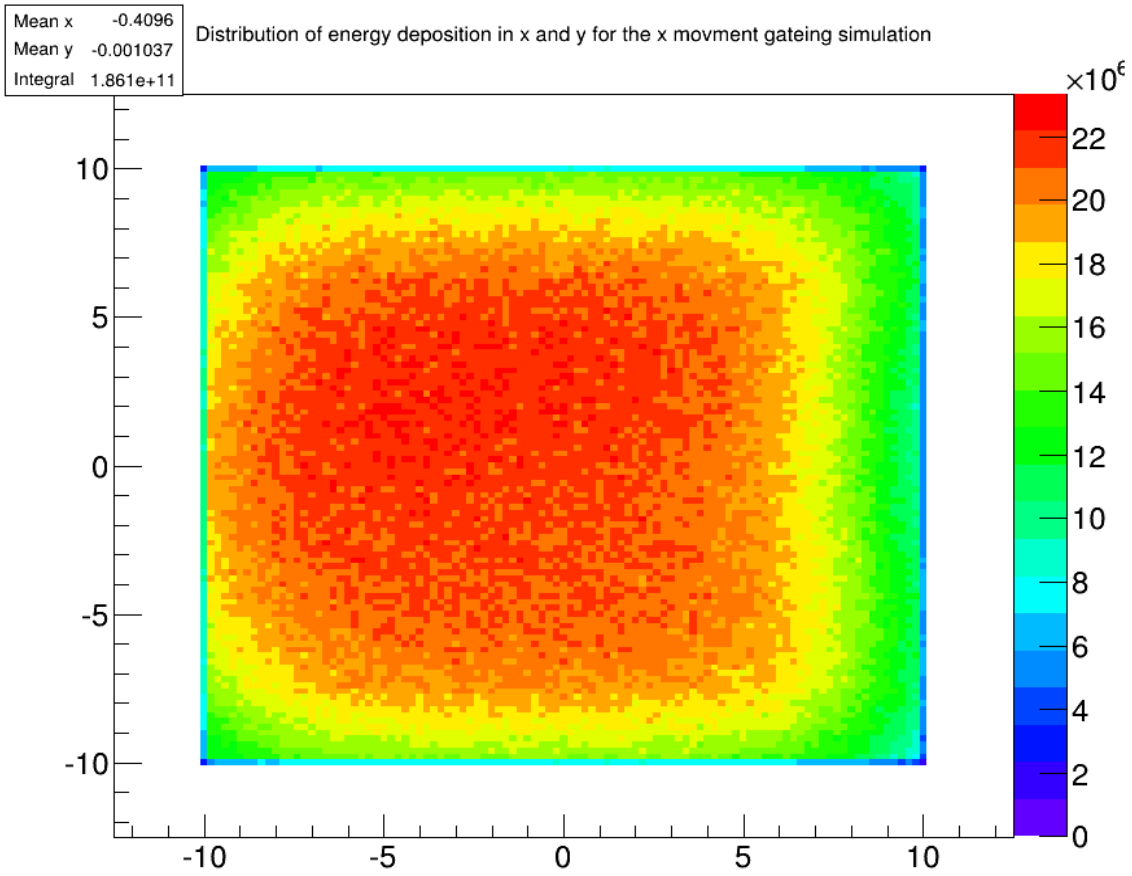

Figure 3.6.1: The distribution of energy deposition in x and y for x movement in the gating window starting as positive.

In this plot we can see that movement in the gating window, which includes both a positive and a negative motion, leads to the energy distribution gaining a greater outwards curving on the negative x side, whilst the side on the positive x side has seemingly gained a slight inward curve in comparison to the static plot. In total the detector registered 98.4% of the total energy registered in the static case. In the CTV only an approximately 6% of the area received less than 90% of the prescribed dose, and the CTV received 98.6% of the energy deposited in the static case. This is a

dramatic improvement over the simulations the previous simulations. This improvement is a combination of the lower average movement in the gating window, the reversing of the movement halfway through the simulation and the resulting lower maximum displacement of the beam spots.

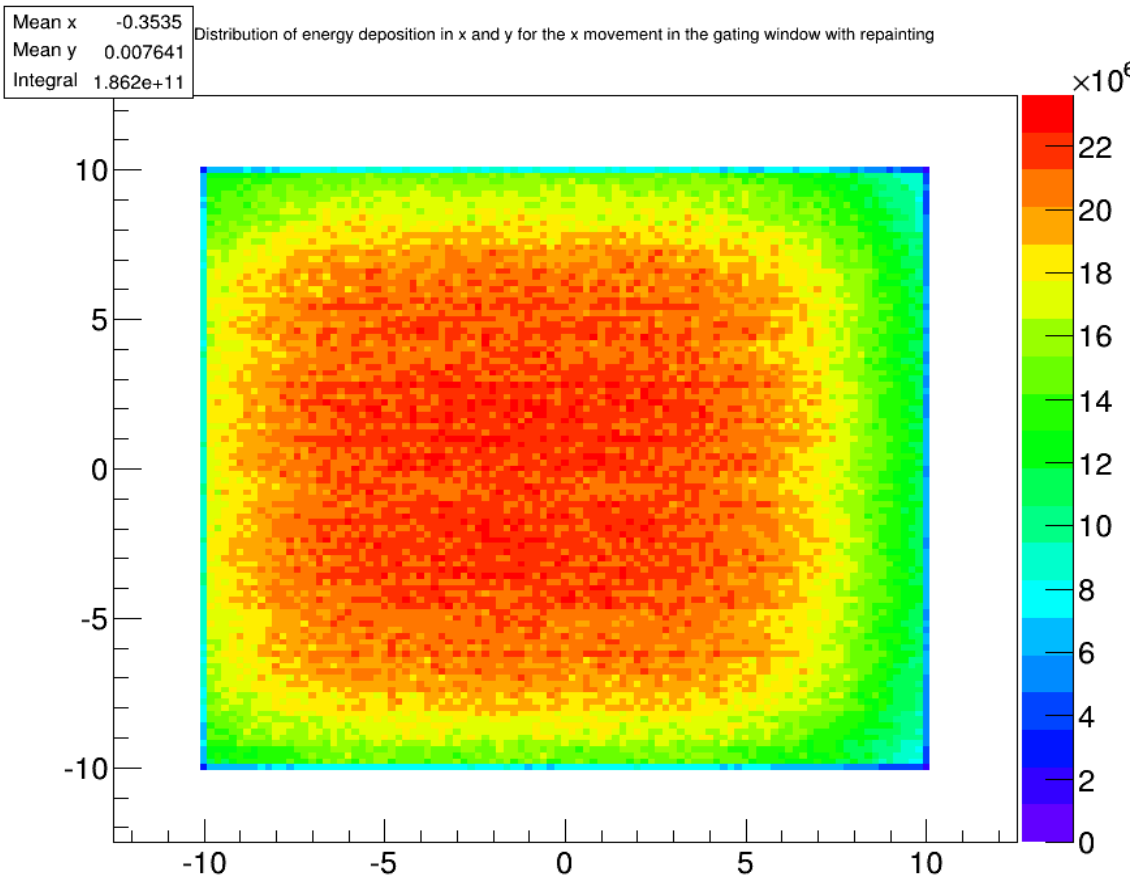

Figure 3.6.2: The distribution of energy deposition in x and y for x movement in the gating window starting as positive with repainting.

When repainting is used in the simulation with movement in the gating window the result is a distribution that is quite similar to the static plot. The only difference is a slight displacement towards negative x and slightly rougher edges. These edges could be a statistical phenomenon or a result of the alternating x movement of the target.

In the CTV the detector registers 99,1% of the total energy deposited in the static case and approximately 3% of the CTV receives less than 90% of the “prescribed dose”

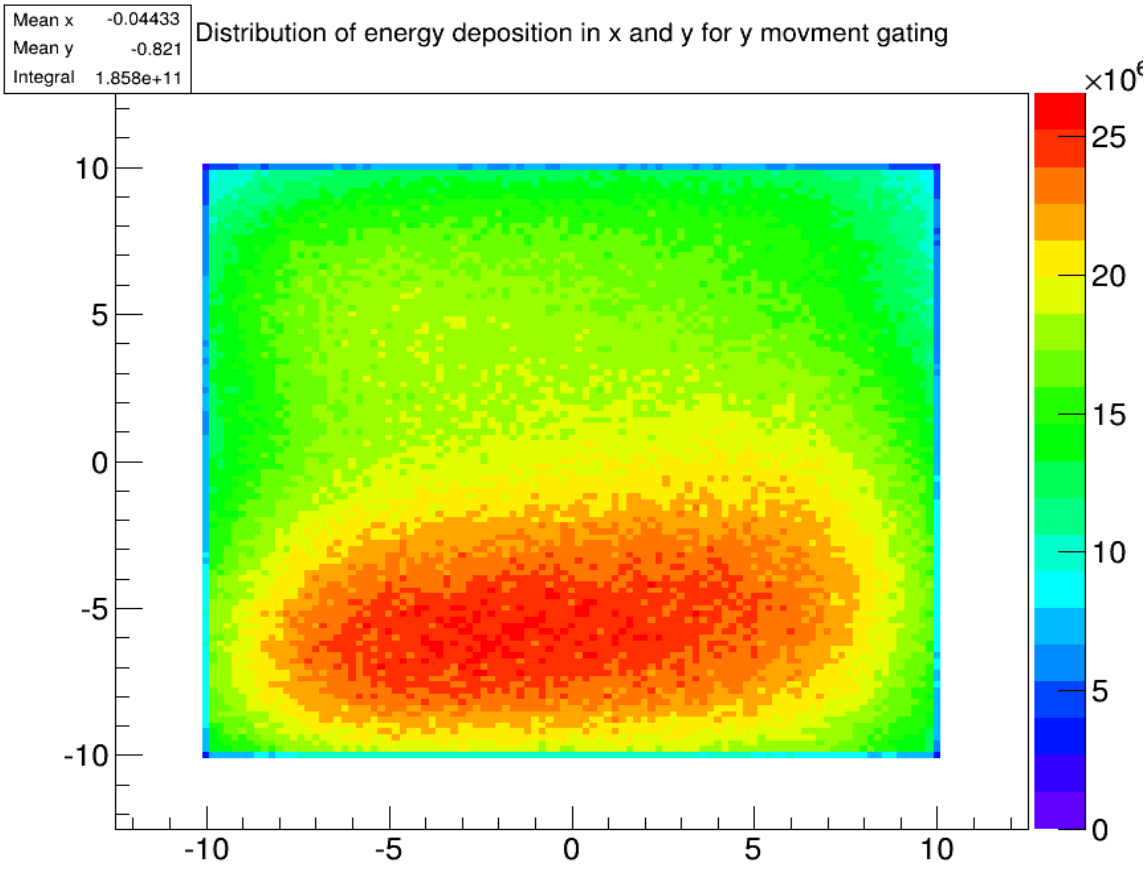

Figure 3.6.3: The distribution of energy deposition in x and y for y movement in the gating window starting as positive.

The plot with movement starting in the positive y direction in the gating window we see that the energy distribution is in some ways similar to the negative y movement distribution in that it has an area of higher energy deposition. The high deposit area have smaller average bin energy deposition than in the negative y movement simulations. There is also a hint of the zig-zag pattern of the positive x movement plot in the slight tail and the tilt towards positive y in the positive x part of the high deposit area.

The CTV received 95.6% of the total energy deposited in the static case but approximately 50% of the CTV received less than 90% of the “prescribed dose” and approximately 36% of the CTV received more than 110% of the “prescribed dose”.

This is the almost the inverse of the situation in the negative y movement simulation, however there is a marked difference in how great the distance in energy deposition is in the high and low deposition areas. With the gating plot reducing the severity of the over and under dosing.

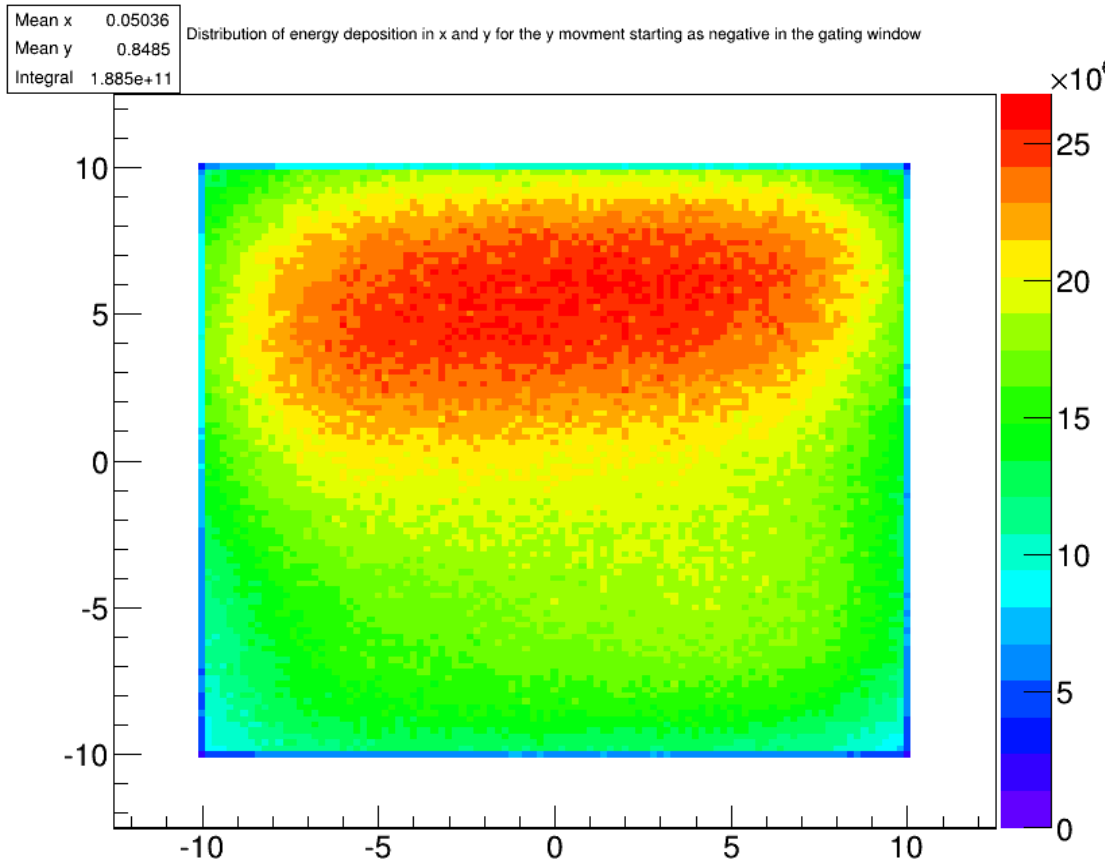

Figure 3.6.4: The distribution of energy deposition in x and y for y movement in the gating window starting as negative.

When simulating the target movement starting as negative in the gating window we get much the same plot as was produced in the previous simulation. The main difference is the inversion of the placement of key areas. The high energy deposit area is now in the positive part of the target and the tilt towards negative y in positive x. This shows that when the target movement changes direction, the effects of both the negative and positive movement on the distribution is applied, regardless of which movement direction is applied first.

The CTV receives in this case 98,1% of the energy deposited in the static simulation, approximately 31% of the CTV received a dose greater than 110% of "prescribed dose" and approximately 48% of the CTV received a dose less than 90% of "prescribed dose". This is slightly better than when the movement starts as positive y.

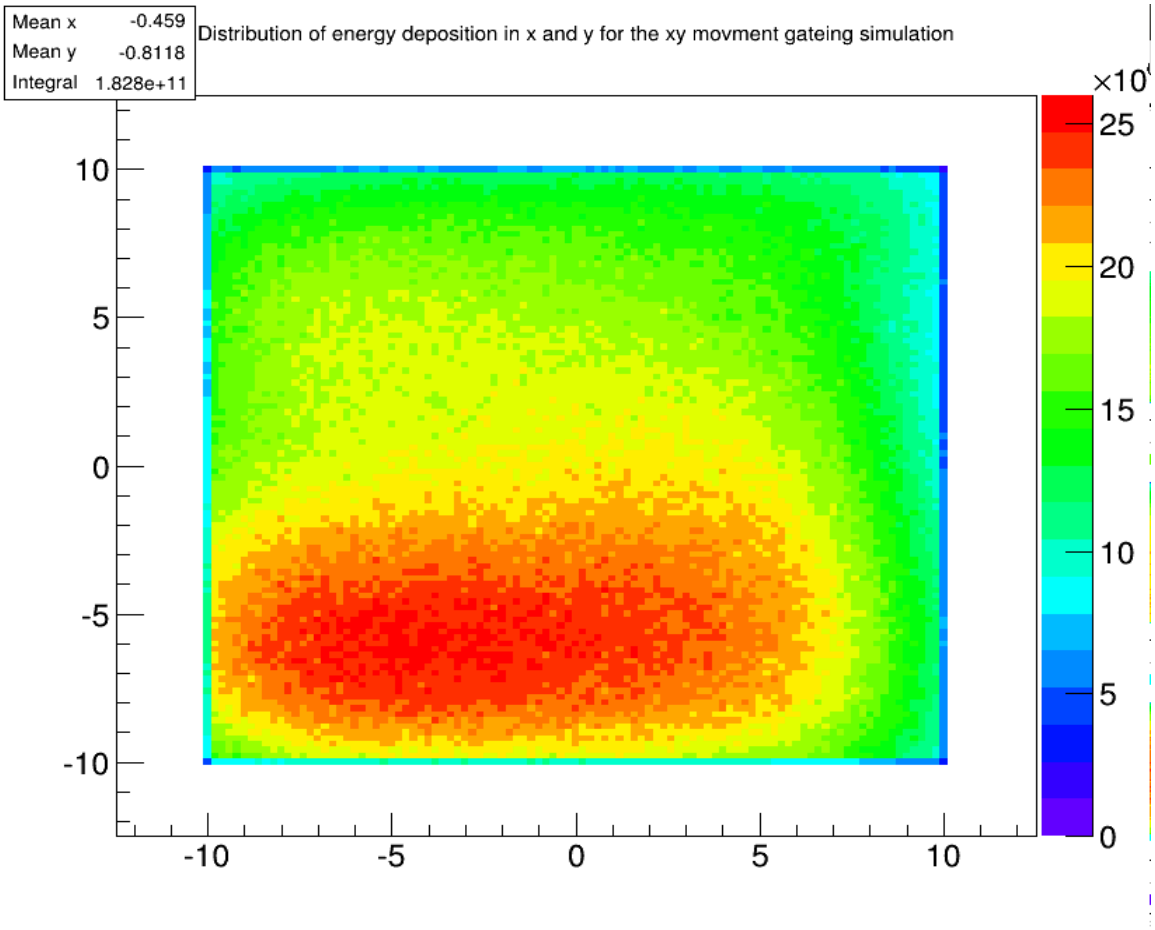

Figure 3.6.5: The distribution of energy deposition in x and y for xy movement in the gating window starting as positive.

As we have seen before, the combination of x movement and y movement leads to a mixing of the traits from the x movement distribution and y movement distribution. We can again see the high deposition in the negative y area with the slight tilt towards positive y in the positive x area. The tail from the positive y movement is now clearly visible but it is unclear if this is the result of the x movement or the slightly lower

maximum bin energy. We can also see that the high deposit area has been displaced slightly towards negative x in accordance with the x movement.

The CTV received 94.9% of the energy deposited in the static simulation, but approximately 46% of the CTV received less than 90% of the “prescribed dose” and approximately 23% received more than 110% of the “prescribed dose”. This leads to a higher percentage of correctly dosed area in this simulation in comparison to the y movement simulation. This is likely due to the displacement of the up tilt of the distribution towards the CTV.

3.7 “Full treatment”

This chapter will present the plots from the simulations including a target motion following the breathing cycle produced by Mohn and Wasbø with a 0,5 sec pause between 1 sec spills.

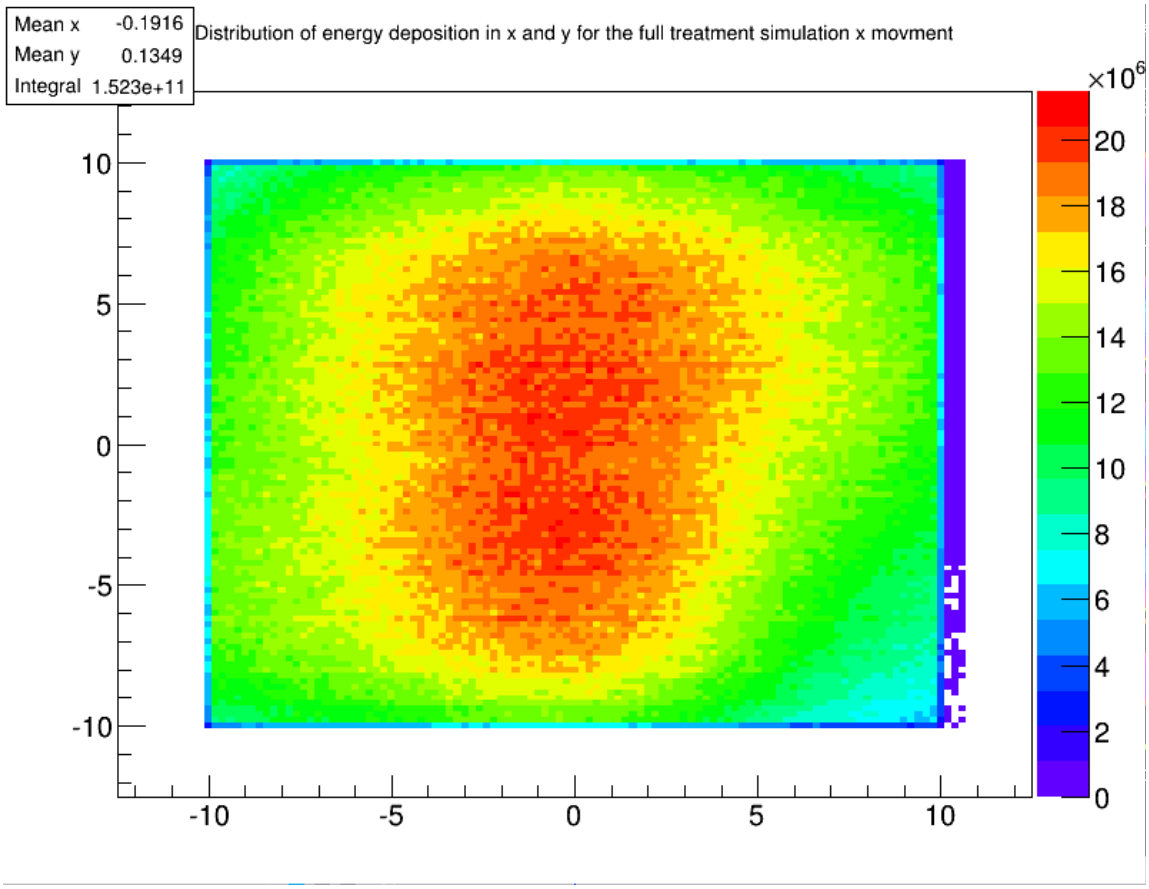

Figure 3.7.1: The distribution of energy deposition in x and y for x movement through the breathing cycle with 10 spills of 1 second with 0.5 seconds pause between spills.

The plot of the full treatment with x movement leaves the high dose area in the middle of the target as in the static case, but much of the dose leaves the target area completely. Only 80.4% of the energy deposited in the static case is registered in the full detector volume. This leads to a decrease of the area of the high dose area and a reduction in the maximum bin energy. The high dose area also has a slight tilt. Towards positive x in the positive y half of the distribution, and towards the negative x in the negative y half of the distribution. This is consistent with the tilt in the

positive x movement plot and the expected result of a negative x movement simulation with reversed scanning direction.

The CTV receives 83.3% of the energy deposited in the static simulation and approximately 62% of the CTV received less than 90% of the “prescribed dose”. This is not far from being the added under-dosage from the positive and negative x movement plots.

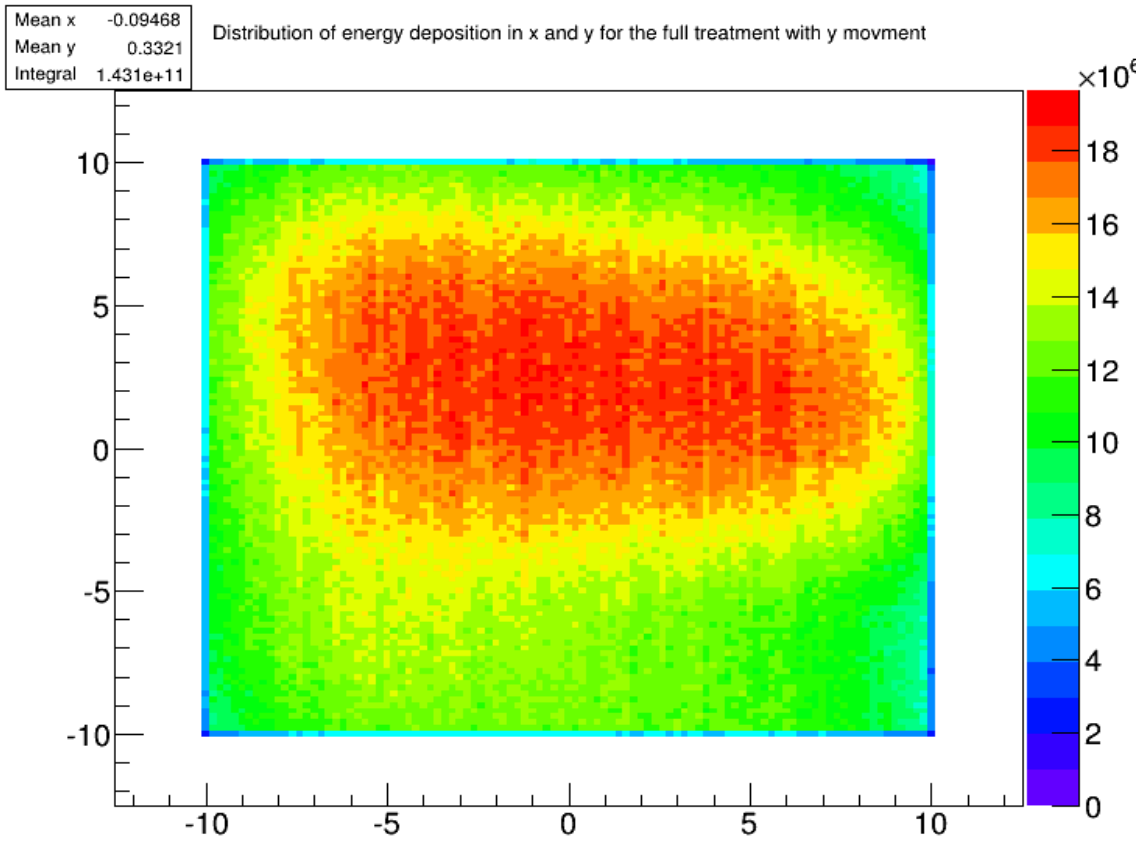

Figure 3.7.2: The distribution of energy deposition in x and y for y movement through the breathing cycle with 10 spills of 1 second with 0.5 seconds pause between spills.

The plot of the full treatment with y movement leaves the high dose area close to the middle of the target as well the distribution has been displaced towards positive y when compared to the static case. The negative x side of the high dose area also ends up being wider than the positive x side. More of the energy has also been deposited

outside of the detector with the detector only registering 75.6% of the energy deposited in the static simulation. Together this leads to almost no bins exceeding 90% of the “prescribed dose” with only 4 bins in the CTV registering more than 19.35 GeV which is insignificant enough to consider 100% of the CTV receiving less than 90% of “prescribed dose”. In total 76.6% of the energy deposited in the CTV in the static case is deposited in the “full treatment” y movement simulation.

3.8 Discussion of Errors

In this chapter the errors associated with the numbers provided will be discussed.

First to be addressed is the errors associated with the total energy deposited in the CTV. The difference between bin energy has been observed to exceed ±1 GeV, see figure 3.1.2. since the average bin energy in the CTV measures at ~ 20 GeV this correlates with an error of ±5%, averaging this over hundreds of bins at the edge of the target area (256 for the CTV) results in an error of ± 1%

This estimate should also hold for the full detector as the dramatic drop of in bin energy at the edge of the detector area (see figure 3.1.2), is caused by the edge bins in the full detector area being halfway outside the detector and therefor only registering ~ 50% of the energy in its area.

The % coverage of the CTV was calculated through manual analysis of the color plots. This leads to a much greater uncertainty than seen in the total energy deposit calculation as the human error must be considered. When calculating the % coverage of the CTV of the same plot, the author has observed variations in % coverage of between 2-3%. The error can therefor be considered to be on the scale of ± 3-4% to account for statistical variations in simulations.

4 Summery and Discussion

In this chapter the results of the simulations will be summarized and discussed, first in separate sections for the basic scanning and the repainting of the basic scans, the gating and the full treatment. In the last section the different techniques will be compared and

4.1 Basic movement and repainting

The results to be discussed in this section was produced by simulating a target moving 1 cm during the irradiation time of 1 second. The results should be considered estimates.

	Basic		
	% under dose	% over dose	% energy deposit
Positive x	32,0%	0,0%	86,6%
Negative x	32,0%	0,0%	89,4%
Positive y	100,0%	0,0%	70,3%
Negative y	38,0%	54,0%	108,3%
Positive xy	100,0%	0,0%	68,0%
Positive x negative y	49,0%	37,0%	90,0%
z movement	100,0%	0,0%	70,2%

Table 4.1.1: The percentage of over and under dosage and energy deposited in the CTV for the basic movement simulations compared to the static simulation.

	Repaint		
	% under dose	% over dose	% energy deposit
Positive x	38,5%	0,0%	87,5%
Non alt x	37,0%	0,0%	87,0%
Positive y	38,0%	0,0%	86,9%
Negative y	40,0%	0,0%	86,4%
Positive xy	67,0%	0,0%	77,0%

Table 4.1.2: The percentage of over and under dosage and energy deposit in the CTV for the repainting simulations with basic movement, compared to the static simulation.

When compared the x movements are almost identical their coverage of the CTV. This is expected as the beam scans in both the positive and negative y direction in these simulations. Though the coverage is poor, with 32% of the CTV not receiving the “prescribed dose”, the movement used in these simulations are on the edge of where it is recommended not to use a scanning technique (Kraus et.al, 2011, see further references therein.), so this is not surprising. And the x movement simulations, or the simulations with the target moving in the positive or negative primary scanning direction, clearly have the best coverage of the CTV of the simple movement simulations. The y directions are widely different, target movement in the positive y direction leads to the dose being stretched out with much of the total energy getting lost outside the simulation detector. This leads to the CTV not receiving the “prescribed dose” in any point. The opposite happens when the target is moved in the negative y direction, the dose is compressed into the positive y half of the target and the CTV receives both a large over dose and a large under dose. With only a small area in between receiving the “prescribed dose”.

In the case of repainting it would seem that the only difference is in which direction the high dose area is displaced. There might be a slight difference between negative y and the other directions, this is likely an effect of the beam having its start and end point (in the case of repainting) in the positive y half of the target. This then resulting in more of the beam spots being close to the edge or outside the target.

More conclusive is the fact that the stretching effect of a positive y movement and the compressing effect of a negative y is removed. The same happens to the tilting effect of the x movement and the distribution retains its shape from the static simulation.

This leads to repainting in these simulations, being of the most benefit in improving the distribution in the y, or secondary scanning, direction.

The non-alternating repainting simulation, while reducing the tilt to the distribution cause by the interplay effect between scanning motion and target motion, does not remove them. This shows that the conformity to the original distribution shape is best preserved with an alternating scanning direction.

As expected the movement along the z-axis lead to a fade out of energy deposition, this because the target moved away from the beams Bragg peak.

While it seems like repainting dose not improve CTV coverage in the case of x movement, it dose improve it greatly in the y movement simulations. The simulations also show that the y-axis, or the secondary scanning direction, is the most negatively affected by movement. The primary scanning direction should therefor coincide with the greatest movement vector.

4.2 Gating

The results to be discussed in this section was produced by simulating a target moving with its minimum movement in the breathing cycle. The simulations encompass both the approach towards the maximum and the decent towards the higher movement part of the breathing cycle. In total the simulation encompass 1 sec of the breathing cycle and during this time the target moves 0,25 cm before changing directions and moving 0,25 cm in the opposing direction. The results should be considered estimates.

	Gating		
	% under dose	% over dose	% energy deposit
x movement	6,0%	0,0%	98,6%
x repanting	3,0%	0,0%	99,1%
positive y start	50,0%	36,0%	95,6%
negative y start	48,0%	31,0%	98,1%
xy movement	46,0%	23,0%	94,9%

Table 4.2.1: The percentage of over and under dosage and energy deposit in the CTV for the simulations of irradiation in the gating window, compared to the static simulation.

Again we can see that the y movement has the most detrimental effect on the dose distribution. The total energy delivered to the seems quite consistent with the exception of the y movement that starts as positive.

The x movement simulation is quite close to being acceptable and the same can then of course be said about the repainting simulation of the x movement in the gating window. Since this is an improvement over the non-repainting simulation. This is not surprising as the magnitude of the motion and the maximum displacement of the target is greatly reduced in the gating window.

And while the dose distribution with y movement dose increase in comparison to the simple movement simulations, they have not improved enough to be considered applicable. The improvement seems to be a combination of less of the total energy getting deposited outside the CTV due to the smaller motion magnitude. And a combining of the stretching out of the distribution from positive y motion and the compression of the distribution from the negative y motion. The more even distribution of the dose in the target seem to support this.

4.3 “Full treatment”

The results to be discussed in this section was produced by simulating a target moving through the breathing cycle produced by Mohn and Wasbø with a 0.5 sec pause between 1 sec spills.

	Full treatment		
	% under dose	% over dose	% energy deposit
x movement	62%	0%	83,3%
y movement	100%	0%	76,6%

Table 4.3.1: The percentage of over and under dosage and energy deposit in the CTV for the “full treatment” simulations, compared to the static simulation.

We can see that the y movement, or movement in the secondary scanning direction, again has the most detrimental effect on the dose coverage of the CTV. An unacceptable dose coverage is expected from these simulations and is consistent with the ICRU recommendation, that scanning techniques are unsuited for targets with motion amplitudes of 10mm or greater. (Kraus et.al, 2011, see further references therein.)

5 Conclusion and Outlook

The objective of this work was to investigate how movement of the target effects on the dose distribution delivered by a scanning particle beam.

The Monte Carlo simulations indicate that movement in the beam direction and in the secondary scanning direction (y), have the most detrimental effect on the dose distribution. Movement in the secondary scanning direction lead to a stretching or spreading out of the dose distribution when the motion of the target was was opposed to the direction of the scanning. This led to much of the beam energy being deposited outside the CTV and outside the detector in the surrounding tissue.

When the target moved with the secondary scanning direction the distribution was displaced and compressed, with movement of the magnitudes applied in these simulations this lead to a high over dosing both in parts of the CTV and in the surrounding tissue.

Since the primary scanning direction (x) is changed several times during the simulations it is expected that the dose distribution should be affected similarly when the target is moved in the positive or negative direction. This is also the result of the simulations. Whether the target moves with the starting direction of the primary scanning direction or against it, the effect is only the direction of the displacement of the deposition and the direction of the tilt.

The repainting simulations indicate that repainting within a spill, will average out the effect of the target and beam moving simultaneously. This lets the dose distribution keep its overall shape and simply be displaced in towards the opposite direction of the target movement. This result is consistent with the purpose of the repainting technique. Which is to contract the interplay effect between these motions. (NuPECC,

2014)

Since the interplay effect are reduced or removed with repainting. The resulting dose distributions have very similar coverage of the CTV regardless if the target was moved in the primary or secondary scanning direction.

The gating simulations show that reducing the magnitude of the target movement improves the delivery of the dose distribution to the target as expected. This was true regardless of the target was moved in the primary beam direction of secondary beam direction.

The results from the simulations with the target starting it's movement in the negative and positive secondary scanning direction (y) are nearly identical, the only difference being the direction of the displacement and tilt of the distribution. Much like the results from the simulations of simple motion in the negative and positive primary scanning direction (x).

With movement in the gating window, the repainting simulation also lead to an increase in coverage of the CTV when the target was moved in the primary scanning direction. The result that repainting leads to a similar distribution and coverage of the CTV regardless of the direction of the target motion, the only difference being the direction of displacement, that was arrived at earlier. Leads to the conclusion that. A repaint simulation of the target moving in the secondary scanning direction in the gating window, should grant similar results to those of repainting of the target moving in the primary beam direction.

The full treatment simulations show motion of the magnitude in the breathing cycle used, lead to an unacceptable dose coverage. This is in line with expectation as it is consistent with the ICRU recommendation, that scanning techniques should not be applied to tumors with motion amplitudes of 10mm or greater. (Kraus et.al, 2011, see further references therein.)

The recent developments in Particle therapy has led it becoming one of the most attractive and sophisticated approaches in the treatment of cancer. This because, the ballistic properties of ions traveling through matter, in combination with the high dose in and the sharp drop-off in dose after the Bragg peak, allows for optimization of the dose to the tumor volume. (NuPECC, 2014)

Recent evaluation by the French ETOILE group, assessed that proton and carbon therapy could be beneficial for approximately 12% and 5% of cancer patients respectively. (NuPECC, 2014) The author feels that these numbers could go up when particle therapy systems that deal with the issue of tumor motion during treatment becomes more prevalent.

Currently a proton beam therapy system using Real-time Tumor-tracking, with the aid of markers, and Spot-Scanning is in use at Hokkaido University in Japan. (Hitach, ltd, 2014)

In the future we might see treatment centers using Carbon ions for treatment and using the capabilities of the accelerator to image the patient on-line or semi on-line with proton CT (theranostics), for beam spot adjustment. This is quite a futuristic vision for particle therapy though and much research will have to be done to determine the possibility of such a treatment system.

References:

E. Badura, H. Brand, H. G. Essel, Th. Haberer, H. Hardel, J. Hoffmann, N. Kurz, P. Liebold, W. Ott, K. Poppensieker, M. Richter *Control System for Cancer Therapy with a Heavy Ion Beam at GSI1,* Gesellschaft fuer Schwerionenforschung mbH, GSI, Planckstr. 1, D-64291 Darmstadt, Germany. https://web-docs.gsi.de/~thdev/rt99/rt99_therapy.html

Introduction to Geant4 last accessed at 20.37 06.05.2015 http://geant4.web.cern.ch/geant4/UserDocumentation/Welcome/IntroductionToGeant4/html/index.html

Physics lists – Use Cases last accessed at 15.21 10.05.2015 http://geant4.cern.ch/support/proc_mod_catalog/physics_lists/useCases.shtml

HIROKI SHIRATO, M.D.,* KEISHIRO SUZUKI, M.D.,* GREGORY C. SHARP, PH.D.,† KATSUHISA FUJITA, R.T.,* RIKIYA ONIMARU, M.D.,* MASAHARU FUJINO, M.D.,* NORIO KATO, M.D.,* YASUHIRO OSAKA, M.D.,* RUMIKO KINOSHITA, M.D.,* HIROSHI TAGUCHI, M.D.,* SHUNSUKE ONODERA, M.D.,* AND KAZUO MIYASAKA, M.D.* *Speed and amplitude of lung tumor motion precisely detected in four-dimensional setup and in real-time tumor-tracking radiationtherapy*, 2006 Int. J. Radiation Oncology Biol. Phys., Vol. 64, No. 4, pp. 1229–1236, Copyright Elsevier Inc.
*Department of Radiology, Hokkaido University School of Medicine, Sapporo, Japan; †Department of Radiation Oncology, Massachusetts General Hospital, Harvard Medical School, Boston, MA

Hokkaido university and Hitachi, ltd, *The PROBEAT-RT Proton Beam Therapy System Incorporating Real-time Tumor-tracking is Approved for Commercial Manufacturing and Sales under Japan's Pharmaceutical Affairs Law*
Treatments to begin using the world's first spot scanning proton beam therapy system equipped with Real-time Tumor-tracking capability Press release 23.09.2014

Hiroki Shirato, Yvette Seppenwoolde, Kei Kitamura, Rikiya Onimura, and Shinichi Shimizu, Intrafractional *Tumor Motion: Lung and Liver*, 2004, *Seminars in Radiation Oncology, Vol 14, No 1 (January), 2004: pp 10-18* Copy right Elsevier Inc.

R. Jadon, C.A. Pembroke, C.L. Hanna, N. Palaniappan, M. Evans, A.E. Cleves, J. Staffurth, *A Systematic Review of Organ Motion and Image-guided Strategies in External Beam Radiotherapy for Cervical Cancer*, Clinical Oncology 26 (2014) 185-196

J Lambert[1,2], N Suchowerska[1,2], D R McKenzie[1] and M Jackson[2], *Intrafractional motion during proton beam scanning*, Phys. Med. Biol. 50 (2005) 4853–4862, [1] School of Physics, The University of Sydney, NSW 2006, Australia, [2] Department of Radiation Oncology, Royal Prince Alfred Hospital, Camperdown, NSW 2050, Australia

K M Kraus[1], E Heath[2] and U Oelfke[1] *Dosimetric consequences of tumour motion due to respiration for a scanned proton beam,* 2011 Phys. Med. Biol. 56(2011) 6563-6581. [1]German Cancer Reaserch Center (DKFZ), [2]Ryerson University, Canada.

K. M. LANGEN, PH.D., AND D. T. L. JONES, PH.D. *Organ motion and its management*, Int. J.

Radiation Oncology Biol. Phys., Vol. 50, No. 1, pp. 265–278, 2001. National Accelerator Centre, Medical Radiation Group, Faure, South Africa

Marcel Marc, *Proton therapy: scattering versus scanning* TALKING POINT
May 28, 2010 on medicalphysicsweb.org http://medicalphysicsweb.org/cws/article/opinion/42793

Nuclear Physics for Medicine, 2014. Nuclear Physics European Collaboration Committee (NuPECC).

SILJE MOHN [1,2] & ELLEN WASBØ [1] Simulation of respiratory motion during IMRT dose delivery, Acta Oncologica, 2011; 50: 935–943. [1]Department of Oncology and Medical Physics, Haukeland University Hospital, Bergen, Norway and [2]Department of Physics, Norwegian University of Science and Technology, Trondheim, Norway

U. Amaldi [1], R. Bonomi, S. Braccini *[2], M. Crescenti [3], A. Degiovanni, M.Garlasché , A. Garonna, G. Magrin [4], C. Mellace [4], P. Pearce [4], G. Pittà [4], P. Puggioni [4], E. Rosso [4], S. Verdu´ Andrés [5], R. Wegner [6], M. Weiss [7], R. Zennaro [8], *Accelerators for hadrontherapy: From Lawrence cyclotrons to linacs,* 2010. TERA Foundation,Via Puccini 11, Novara, Italy

YTRE-HAUGE, KRISTIAN. 2013 *Measurementsand Monte Carlo Simulationsof Neutron Doses from Radiation Therapy with Photons, Protons and Carbon Ions* Ph.D., University of Bergen

Yupeng Li, Laleh Kardar, Xiaoqiang Li, Heng Li, Wenhua Cao, Joe Y. Chang, Li Liao, Ronald X. Zhu, Narayan Sahoo, Michael Gillin, Zhongxing Liao, Ritsuko Komaki, James D. Cox, Gino Lim, Xiaodong Zhang, *On the interplay effects with proton scanning beams in stage III lung cancer*, 2014 Med. Phys. 41 (2)